Author(s): Jarkko Niiranen, Sergei Khakalo, Viacheslav Balobanov, Antti H. Niemi

Title: Variational formulation and isogeometric analysis for fourth-order boundary value problems of gradient-elastic bar and plane strain/stress problems

Year: 2016

Version: preprint

Please cite the original version:

Jarkko Niiranen, Sergei Khakalo, Viacheslav Balobanov, Antti H. Niemi. Variational formulation and isogeometric analysis for fourth-order boundary value problems of gradient-elastic bar and plane strain/stress problems. Computer Methods in Applied Mechanics and Engineering, 308:182-211, August 2016. DOI: 10.1016/j.cma.2016.05.008

Variational formulation and isogeometric analysis for fourth-order boundary value problems of gradient-elastic bar and plane strain/stress problems

Jarkko Niiranen*, Sergei Khakalo, Viacheslav Balobanov, Antti H. Niemi

Aalto University, Department of Civil and Structural Engineering
P.O. Box 12100, 00076 AALTO, Finland

Abstract

The fourth-order boundary value problems of one parameter gradient-elastic bar and plane strain/stress models are formulated in a variational form within an H^2 Sobolev space setting. For both problems, the existence and uniqueness of the solution is established by proving the continuity and coercivity of the associated symmetric bilinear form. For completeness, the full sets of boundary conditions of the problems are derived and, in particular, the new types of boundary conditions featured by the gradient-elastic models are given the additional attributes *singly* and *doubly*. By utilizing the continuity and coercivity of the continuous problems, corresponding error estimates are formulated for conforming Galerkin formulations. Finally, numerical results, with isogeometric C^{p-1}-continuous discretizations for NURBS basis functions of order $p \geq 2$, confirm the theoretical results and illustrate the essentials of both static and vibration problems.

Keywords: Gradient elasticity, Bar, Plane strain/stress, Variational formulation, Existence and Uniqueness, Isogeometric analysis, Error estimates
PACS: 46.70.-p, 46.70.Hg, 46.70.De, 46.15.-x, 46.15.Cc, 46.25.-y, 46.25.Cc
2000 MSC: 74A60, 74K10, 74K15, 74K20, 35J35, 35J40, 65M12, 65M15, 65M60, 74S05

*Corresponding author: jarkko.niiranen@aalto.fi

1. Introduction

Classical continuum theories, such as theories of linear or nonlinear elasticity and plasticity, have been widely used in various fields of science and engineering for modelling solids and structures. The ability of classical continuum theories for describing multi-scale phenomena, is very limited, however. On the other hand, theories and methods for studying small-scale phenomena, such as molecular dymanics, are often inefficient in many applications eventually ruled by macro-scale conservations laws. This has raised a motivation for further development of single-scale continuum mechanics which have been extended towards multi-scale capabilities still preserving the most characteristic advantages of their homogenizing nature [1, 2, 3].

In the current work, we concentrate on a single-parameter simplified theory (proposed in [4, 5] in the 1990s) of the gradient elasticity theory of Form II derived by Mindlin (in the landmark paper [6] in the 1960s). However, our theoretical results can be extended to more general multi-parameter models of Form II and I in a natural way. Regarding experimental background and applications of gradient elasticity theories, we refer to the discussion in [7, 8, 9]. For determining the material parameters of the models, we refer to [10, 7, 11].

Within the classical elasticity theory, the engineering bar model as well as plane stress and plane strain models lead to second-order partial differential equations. Within the theory of gradient elasticity, instead, these models lead to fourth-order governing equations [12, 13]. In particular, this fact complicates the numerical methods applied for solving the corresponding boundary value problems since higher order derivatives in Euler equations imply higher order (weak) derivatives in the corresponding variational formulations. Accordingly, the related trial and test functions of Galerkin methods, for instance, have to meet higher regularity conditions. For fourth-order Euler equations, in particular, C^1 continuity is required for satisfying the H^2 regularity in the weak form. Isogeometric analysis in the Galerkin sense (initiated in [14]) which provides straightforward C^{p-1} discretizations, for NURBS basis functions of order $p \geq 2$, appears as an even more attractive method for higher-order boundary value problems (see [15, 16, 17, 18], for instance) than for lower order formulations of the classical elasticity theory (as [19, 20], for instance).

Solvability of gradient-elastic problems has been addressed in few studies only, as in [5]. Uniqueness of the solution, in particular, has been discussed

in the context of analytical solutions for a one-dimensional model problem in [21, 22] by introducing the term "sign paradox". The discussion on this issue have been extended in [7] for a class of more general constitutive tensors of gradient elasticity. A more theoretical analysis have been accomplished in [23] for solvability of two parameter fourth-order gradient elasticity problems written as a mixed variational formulation in an H^1 Sobolev space framework in order to utilize the Babuska–Brezzi theory. In this paper, we focus on the variational formulation and its solvability, i.e., existence and uniqueness, of the gradient-elastic bar and plane strain/stress problems corresponding to the fourth-order boundary value problems presented in [21, 12, 13, 24, 3]. Accordingly, we prove the well-posedness of the corresponding displacement based variational formulations within H^2 Sobolev space settings. In contrast to classical problems governed by fourth order partial differential equations, such as the Kirchhoff plate problem commanded by the biharmonic equation, problems of gradient elasticity are essentially affected by the gradient parameters associated to the higher order derivatives. Our proofs are established for clamped boundaries but they can be extended to other boundary condition types as well. Regarding boundary conditions, in particular, this paper recalls and identifies two different types of clamped and free boundary conditions and gives them additional attributes *singly* and *doubly*. Furthermore, corner conditions often omitted in the literature are derived as well. Altogether, our formalism provides a consistent framework for both variational and non-variational general-purpose numerical approximation methods.

Regarding numerical methods for gradient elasticity and applications, only a limited number of model problems with simple geometries and non-general boundary conditions have been solved, and mostly by analytical means (see [12, 24, 13, 3, 25, 26]). In particular, for numerical methods capable of solving general geometries and different boundary conditions, the literature is very limited, even for bar and plane problems. First, in [27], a group of C^0-continuous elements based on a mixed formulation have been proposed; second, in [28], a consistent and stable discontinuous Galerkin method have been formulated, theoretically analyzed and verified for a shear layer problem of strain gradient elasticity (formally identical to the bar problem); third, in [29, 30], a couple of C^1-continuous elements have been introduced; fourth, in [31], a C^0-continuous approach have been applied. More recently, [16] has benchmarked static plane gradient elasticity problems by C^{p-1}-continuous isogeometric discretizations, with $p \geq 2$ referring to the order of NURBS basis functions. Finally, in [32], three-dimensional problems of

Toupin's gradient elasticity theory at finite strains have been solved by applying H^2-conforming, i.e., at least C^1-continuous, isogeometric discretizations – including the one-dimensional bar problem with infinitesimal strains as a verification benchmark for convergence studies. All of the aforementioned articles concentrate on the static problems of gradient elasticity. Furthermore, only [28] concentrates on formulating and analyzing the problems and related methods within a theoretical framework. In this paper, we fill this gap present on the theoretical side for the continuous formulations and the corresponding conforming Galerkin methods, for both bar and plane gradient elasticity problems. In addition, our numerical benchmarks and examples confirm the theoretical results and clarify the effect of the gradient terms on both static and vibration problems, the latter being practically impossible to analyse without a numerical approach for plane strain/stress problems.

This paper is organized as follows: In Section 2, we introduce our notation by recalling the variational formulations of the gradient-elastic bar model as well as plane stress and plane strain models. For completeness, in Section 3, the principle of virtual work is applied for deriving the boundary conditions and governing equations. Section 4 is devoted to the stability analysis of the corresponding variational formulations. Section 5 is written for presenting the isogeometric Galerkin methods and convergence analysis. Finally, in Section 6, numerical benchmarks and examples are analysed. Proofs are given in the Appendix.

2. Continuum models

For clarity and introducing the notation, we first briefly recall the internal virtual work expression and corresponding constitutive relations for the theory of a linearly isotropic gradient-elastic continuum. Second, we describe the physical setting of the corresponding problems of bars as well as plane stress and plane stress assumptions.

2.1. Strain-gradient elasticity

Let us first consider the virtual work expression for a three-dimensional elastic continuum with a deformable micro-structure (see [6], Eq. (11.7)) written over a body $\mathcal{B} \subset \mathbb{R}^3$ in the form

$$\delta W_{\text{int}} = \int_{\mathcal{B}} \boldsymbol{\sigma} : \boldsymbol{\varepsilon}(\delta \boldsymbol{u}) \, \mathrm{d}\mathcal{B} + \int_{\mathcal{B}} \boldsymbol{\tau} \vdots \boldsymbol{\gamma}(\delta \boldsymbol{u}) \, \mathrm{d}\mathcal{B}, \tag{2.1}$$

where : and $\vdots$ denote the contractions for second and third-order tensors, respectively. Applying Einstein's summation convention, these products are defined as

$$\boldsymbol{\sigma} : \boldsymbol{\varepsilon} = \sigma_{ij}\epsilon_{ij}, \quad \boldsymbol{\tau} \vdots \boldsymbol{\gamma} = \tau_{ijk}\gamma_{ijk}. \tag{2.2}$$

As usual, in the linear elasticity theory the classical Cauchy stress tensor $\boldsymbol{\sigma} : \mathcal{B} \to \mathbb{R}^{3\times3}$ is assumed to be related to its work conjugate linear strain tensor $\boldsymbol{\varepsilon} : \mathcal{B} \to \mathbb{R}^{3\times3}$,

$$\boldsymbol{\varepsilon}(\boldsymbol{u}) = \frac{1}{2}\big(\boldsymbol{\nabla u} + (\boldsymbol{\nabla u})^T\big), \tag{2.3}$$

through the generalized Hooke's law

$$\boldsymbol{\sigma} = 2\mu\boldsymbol{\varepsilon} + \lambda \mathrm{tr}\,\boldsymbol{\varepsilon}\boldsymbol{I}, \tag{2.4}$$

with the Lame material parameters $\mu = \mu(x, y, z)$ and $\lambda = \lambda(x, y, z)$, and with $\boldsymbol{I}$ denoting the (second order) identity tensor. Above, the displacement field is denoted by $\boldsymbol{u} : \mathcal{B} \to \mathbb{R}^3$ and the (second order) tensor-valued gradient operator is denoted by $\boldsymbol{\nabla}$, or later with the index notation as $u_{i,j}$ where indeces i and j refer to x, y and z components of $\boldsymbol{u}$, or the corresponding partial derivatives when placed after the comma.

The (third order) micro-deformation gradient tensor $\boldsymbol{\gamma} : \mathcal{B} \to \mathbb{R}^{3\times3\times3}$ follows Mindlin's Form II model [6] based on Toupin's generalization of the couple stress theory [33, 34] (see Mindlin's Form I model as well):

$$\boldsymbol{\gamma} = \boldsymbol{\nabla\varepsilon}. \tag{2.5}$$

The (third-order) double stress tensor $\boldsymbol{\tau} : \mathcal{B} \to \mathbb{R}^{3\times3\times3}$, in turn, is the corresponding work conjugate quantity and it is related to $\boldsymbol{\gamma}$ by a set of additional material parameters besides the two Lame parameters. In this context, $\boldsymbol{\nabla}$ denotes the (third-order) tensor valued-gradient operator with the index notation counterpart $\epsilon_{ij,k}$.

The simplest variant of Mindlin's strain gradient elasticity theory with constant Lame parameters has been proposed in [4, 35] by defining the double stress tensor in the form

$$\boldsymbol{\tau} = g^2\boldsymbol{\nabla\sigma}, \tag{2.6}$$

with g denoting the gradient-elastic modulus, or the volumetric strain energy gradient modulus, which describes the length scale of the micro-structure of the material. In general, g could be considered to be a non-constant material parameter, i.e., $g = g(x, y, z)$. Typically, however, g is assumed to be constant, which is our assumption as well.

Remark 1. *In the simplest variant of Mindlin's strain gradient model adopted in* (2.6) *(with* (2.5)*), the double stress tensor $\boldsymbol{\tau}$ is related to the strain gradient tensor $\boldsymbol{\nabla\varepsilon}$ by the two Lame parameters and the additional gradient parameter (in the case of isotropic materials), whereas in Mindlin's Form II model this relation is defined by five independent gradient parameters (see [6], Eq. (11.6)$_2$), say, by a constitutive tensor $\boldsymbol{G}$ as $\boldsymbol{\tau} = \boldsymbol{G}\boldsymbol{\nabla\varepsilon}$. Therefore, our theoretical results of Section 4 could be extended to Form II model in a natural way (see Remark 4).*

Now, substituting equations (2.6) and (2.5) into the virtual work expression (2.1) yields [25]

$$\delta W_{\text{int}} = \delta W_{\text{int}}^{\text{c}} + \delta W_{\text{int}}^{\nabla} = \int_{\mathcal{B}} \boldsymbol{\sigma} : \boldsymbol{\varepsilon}(\delta\boldsymbol{u}) \, \mathrm{d}\mathcal{B} + \int_{\mathcal{B}} g^2 \boldsymbol{\nabla\sigma} \vdots \boldsymbol{\nabla\varepsilon}(\delta\boldsymbol{u}) \, \mathrm{d}\mathcal{B}, \quad (2.7)$$

This energy expression will be used for the weak formulation below and taken as the starting point for deriving the boundary conditions of the problem. Here and below, superscript g can be considered to refer to the term "gradient-elastic", or to the gradient-elastic modulus as a parameter (with $g = 0$ giving the classical case, often written without the superscript 0, however).

Applying integration by parts once (cf. (7.2) below for details) for the second term in (2.7) (or already in (2.1) with (2.5)) gives the total Cauchy stress tensor of the gradient-elastic framework as a combination of the classical and double stress tensor in the form

$$\boldsymbol{\sigma}^g = \boldsymbol{\sigma} - \mathbf{div}\, \boldsymbol{\tau} = (1 - g^2\Delta)\boldsymbol{\sigma}, \quad (2.8)$$

giving the name Laplacian-based gradient elasticity [3] referring to the (scalar) Laplace operator Δ acting on the classical stress tensor in the additional gradient-elastic stress contribution. Above, **div** denotes the vector-valued divergence operator.

The external virtual work possesses non-classical terms (forming $\delta W_{\text{ext}}^{\nabla}$) related to so-called body double force (second order) tensor $\boldsymbol{\Phi}$, surface double

force (vector) $\boldsymbol{r}$ and edge force (vector) $\boldsymbol{t}_l$, beside the classical body and surface forces (vectors) $\boldsymbol{f}$ and $\boldsymbol{t}$ (forming $\delta W^{\mathrm{c}}_{\mathrm{ext}}$) [36, 37]:

$$\begin{aligned}\delta W_{\mathrm{ext}} &= \delta W^{\mathrm{c}}_{\mathrm{ext}} + \delta W^{\nabla}_{\mathrm{ext}} \\ &= \int_{\mathcal{B}} \boldsymbol{f} \cdot \delta\boldsymbol{u}\,\mathrm{d}\mathcal{B} + \int_{\partial\mathcal{B}} \boldsymbol{t} \cdot \delta\boldsymbol{u}\,\mathrm{d}\partial\mathcal{B} \\ &\quad + \sum_l \int_l \boldsymbol{t}_l \cdot \delta\boldsymbol{u}\,\mathrm{d}l + \int_{\mathcal{B}} \boldsymbol{\Phi} : \boldsymbol{\nabla}\delta\boldsymbol{u}\,\mathrm{d}\mathcal{B} + \int_{\partial\mathcal{B}} \boldsymbol{r} \cdot (\boldsymbol{\nabla}\delta\boldsymbol{u})\boldsymbol{n}\,\mathrm{d}\partial\mathcal{B} \end{aligned} \tag{2.9}$$

where the outward unit normal to the boundary surface $\partial\mathcal{B}$ is denoted by $\boldsymbol{n}$ and l stands for sharp edges of the boundary surface. For simplicity, however, we omit the non-classical external loadings in our analysis by assuming that $\boldsymbol{\Phi} = \boldsymbol{0}$. The surface forces and surface double force will be addressed in the context of boundary conditions.

Finally, for analysing vibrations within the current gradient elasticity theory an additional gradient parameter introducing a micro-inertia term has been proposed [36, 13] in order to achieve a physically satisfactory dispersion relation for a large range of wave numbers. The variation of the kinetic energy is then written in the form

$$\delta \int_T W_{\mathrm{kin}}\,\mathrm{d}t = -\int_T \Big(\int_{\mathcal{B}} \rho\ddot{\boldsymbol{u}} \cdot \delta\boldsymbol{u}\,\mathrm{d}\mathcal{B} + \int_{\mathcal{B}} \gamma^2\rho\boldsymbol{\nabla}\ddot{\boldsymbol{u}} : \boldsymbol{\nabla}\delta\boldsymbol{u}\,\mathrm{d}\mathcal{B}\Big)\,\mathrm{d}t \tag{2.10}$$

with T denoting a time interval and ρ denoting the mass density.

2.2. Axially loaded gradient elastic rod

Let us consider a cylinder-like three-dimensional body

$$\mathcal{P} = A \times \Omega, \tag{2.11}$$

where $\Omega = (0, L)$ denotes the central axis of the structure with L standing for the length of the structure, whereas $A \subset \mathbb{R}^2$ denotes a cross-section of the structure, with $\mathrm{diam}(A) \ll L$.

First of all, let us assume that the material properties and body forces as well as (both static and kinematic) boundary conditions on the end point cross-sections are uniformly distributed. Furthermore, it is assumed that only the axial component of the body load $\boldsymbol{f} : \mathcal{P} \to \mathbb{R}^3$, and possible boundary tractions, are present.

In the so called *engineering bar* model for axially loaded rods, the kinematical dimension reduction assumptions [38] presuppose the displacement field $\boldsymbol{u} = \boldsymbol{u}(u_x, u_y, u_z)$ of the form

$$u_x = u(x), \quad u_y = 0, \quad u_z = 0, \tag{2.12}$$

which implies that the axial strain $\epsilon_{xx} = u'(x)$ is the only nonzero component of the strain tensor. Regarding the constitutive relation (2.4), the engineering model (see [38]) assumes that $\sigma_{xx} = E\epsilon_{xx}$ is the only non-zero component of the stress tensor, with Young's modulus E given in terms of the Lame parameters:

$$E = \frac{\mu(3\lambda + 2\mu)}{\lambda + \mu}. \tag{2.13}$$

The internal virtual work expression (2.7) then reduces to

$$\delta W_{\text{int}} = \int_\Omega A\sigma_{xx}\, \epsilon_{xx}(\delta u)\, \mathrm{d}x + \int_\Omega A g^2 \sigma'_{xx}\, \epsilon'_{xx}(\delta u)\, \mathrm{d}x. \tag{2.14}$$

Accordingly, in view of (2.8), the constitutive equations for the corresponding gradient-elastic rod model reduce to the stress-strain relation in the axial direction written as

$$\sigma^g_{xx} = (1 - g^2 \frac{\mathrm{d}^2}{\mathrm{d}x^2}) E\epsilon_{xx}. \tag{2.15}$$

Finally, with the assumed external loading $\boldsymbol{f} = (f(x), 0, 0)$, with a simplifying assumption $\boldsymbol{t} = \boldsymbol{0} = \boldsymbol{t}_l$, the external virtual work (2.9) can be written as

$$\delta W^{\text{c}}_{\text{ext}} = \int_{\mathcal{P}} \boldsymbol{f} \cdot \delta\boldsymbol{u}\, \mathrm{d}\mathcal{P} = \int_\Omega A f\, \delta u\, \mathrm{d}x. \tag{2.16}$$

2.3. Plane gradient elasticity

Plane strain model. Let us consider a cylinder-like structure which occupies a three-dimensional body

$$\mathcal{P} = \Omega \times (-\frac{t}{2}, \frac{t}{2}), \tag{2.17}$$

where $t \gg \text{diam}(\Omega)$ denotes the length, or thickness, of the structure and the domain $\Omega \subset \mathbb{R}^2$ denotes a cross section of the structure. Let us denote the

top and bottom surfaces and the lateral boundary of the body, respectively, as

$$\partial\mathcal{P}_- = \Omega \times \{-\frac{t}{2}\}, \quad \partial\mathcal{P}_+ = \Omega \times \{\frac{t}{2}\}, \quad \partial\mathcal{P}_\mathrm{L} = \partial\Omega \times (-\frac{t}{2}, \frac{t}{2}). \tag{2.18}$$

The boundary curve $\partial\Omega$ can be assumed to be piecewise smooth (satisfying the so called cone condition providing positive interior angles for all vertices [39, 40]).

Next, we assume that the material properties and body forces as well as boundary conditions on $\partial\mathcal{P}_\mathrm{L}$ do not vary in the thickness direction. Furthermore, it assumed that only the in-plane components of the body load $\boldsymbol{f} : \mathcal{P} \to \mathbb{R}^3$ and possible boundary tractions are present.

Finally, let us denote the three-dimensional displacement field of the body by $\boldsymbol{u} : \mathcal{P} \to \mathbb{R}^3$, $\boldsymbol{u} = (u_x, u_y, u_z)$, where $u_i = u_i(x, y, z)$, $i = x, y, z$ with the global Cartesian coordinates x, y, z. The displacement component of the thickness direction is assumed to be fixed on the end surfaces of the body, i.e., $u_z = 0$ on $\partial\mathcal{P}_+ \cup \partial\mathcal{P}_-$.

Under these assumptions, the dimension reduction hypotheses of the *plane strain* model allow us to write the displacement field as [41]

$$u_x = u_x(x, y), \quad u_y = u_y(x, y), \quad u_z = 0, \tag{2.19}$$

which, by to (2.3), implies that $\epsilon_{iz} = 0$, $i = x, y, z$ reducing the strain tensor into two dimensions. Accordingly, in view of (2.4), the condition $\epsilon_{zz} = 0$ implies that $\sigma_{zz} = \nu(\sigma_{xx} + \sigma_{yy})$, which means that the generalized Hooke's law can be restricted to the planar components. Therefore, the virtual work expression (2.7) can be applied with $\boldsymbol{u} = (u_x(x, y), u_y(x, y))$ denoting now the in-plane displacement vector, $\boldsymbol{\varepsilon}$ and $\boldsymbol{\sigma}$ denoting the corresponding restrictions of the strain and stress tensors, and $\boldsymbol{\nabla}$ including partial derivatives with respect to x and y only:

$$\delta W_\mathrm{int} = t \int_\Omega \boldsymbol{\sigma} : \boldsymbol{\varepsilon}(\delta\boldsymbol{u}) \,\mathrm{d}\Omega + t \int_\Omega g^2 \boldsymbol{\nabla}\boldsymbol{\sigma} \vdots \boldsymbol{\nabla}\boldsymbol{\varepsilon}(\delta\boldsymbol{u}) \,\mathrm{d}\Omega, \tag{2.20}$$

where the thickness is assumed to be constant and the constitutive relation

$$\boldsymbol{\sigma} = \boldsymbol{E}\,\boldsymbol{\varepsilon}(\delta\boldsymbol{u}) \tag{2.21}$$

is defined by representing the symmetric and positive definite in-plane elasticity tensor $\boldsymbol{E} : \Omega \to \mathbb{R}^{2\times2\times2\times2}$ following (2.4) and the plane elasticity model considered.

In view of (2.8), the constitutive equations for the gradient-elastic plane strain model reduce to the planar components:

$$\sigma^g_{xx} = (1 - g^2\Delta)\frac{E}{(1+\nu)(1-2\nu)}((1-\nu)\epsilon_{xx} + \nu\epsilon_{yy}), \tag{2.22}$$

$$\sigma^g_{yy} = (1 - g^2\Delta)\frac{E}{(1+\nu)(1-2\nu)}((1-\nu)\epsilon_{yy} + \nu\epsilon_{xx}), \tag{2.23}$$

$$\sigma^g_{xy} = (1 - g^2\Delta)\frac{E}{1+\nu}\epsilon_{xy}, \tag{2.24}$$

with the material parameters, Young's modulus E and Poisson's ratio ν, given in terms of the Lame parameters by (2.13) and

$$\nu = \frac{\lambda}{2(\lambda+\mu)}, \tag{2.25}$$

where the shear modulus μ is often denoted by G in engineering literature.

Plane stress model. Let us consider a three-dimensional thin planar plate, or membrane, structure

$$\mathcal{P} = \Omega \times (-\frac{t}{2}, \frac{t}{2}), \tag{2.26}$$

where the domain $\Omega \subset \mathbb{R}^2$ denotes the midsurface of the membrane and $t \ll \text{diam}(\Omega)$ denotes the thickness of the membrane. For simplicity, the thickness is assumed to be constant.

As above, we assume that the material properties and body forces as well as the surface tractions do not vary in the thickness direction. Furthermore, it is assumed that only the in-plane components of the body load $\boldsymbol{f} : \mathcal{P} \to \mathbb{R}^3$, and the boundary tractions, are present, while the top and bottom surfaces $\partial\mathcal{P}_+$ and $\partial\mathcal{P}_-$ are assumed to be free of loads. Regarding the kinematic boundary conditions in the thickness direction, is assumed that u_z is an odd function of z on $\partial\mathcal{P}$, where the Cartesian coordinate system is placed in the center of gravity of the body with its origin fixed to the midsurface. With these assumptions, the plate is assumed to be in *streching* state rather than *bending* state (see [37] for more details on plate bending problems).

Under these assumptions, the *plane stress* hypothesis $\sigma_{iz} = 0$, $i = x, y, z$ is appropriate. Accordingly, in view of (2.4), the conditions $\sigma_{iz} = 0$ with $i = x, y$ imply that $\epsilon_{iz} = 0$, $i = 1, 2$, whereas the condition $\sigma_{zz} = 0$ implies

that $\epsilon_{zz} = -\nu(\epsilon_{xx} + \epsilon_{yy})/(1-\nu)$, which means that the generalized Hooke's law can be restricted to the planar components.

In view of (2.8), the constitutive equations for the gradient-elastic plane stress model can be written in component form as

$$\sigma^g_{xx} = (1 - g^2\Delta)\frac{E}{1-\nu^2}(\epsilon_{xx} + \nu\epsilon_{yy}), \tag{2.27}$$

$$\sigma^g_{yy} = (1 - g^2\Delta)\frac{E}{1-\nu^2}(\epsilon_{yy} + \nu\epsilon_{xx}), \tag{2.28}$$

$$\sigma^g_{xy} = (1 - g^2\Delta)\frac{E}{1+\nu}\epsilon_{xy}, \tag{2.29}$$

Remark 2. *It should be noticed, that with the assumptions above the plane stress model is not a true dimension reduction model since the stress, strain and displacement fields can still depend on z coordinate. The z dependency can be ignored by introducing the generalized plane stress formulation introducing the mean values*

$$\bar{u}_i(x,y) = \frac{1}{t}\int_{-t/2}^{t/2} u_i(x,y,z)\,\mathrm{d}z, \tag{2.30}$$

which implies that $\bar{u}_3 = 0$ since u_3 is an odd function of z due to the assumed loading symmetry with respect to the midsurface (see [41] for further details, and the quasi-plane stress formulation discussed in [42]).

As long as the plane elasticity model considered is a truly planar dimension reduction model, it is enough to consider only one model with its constitutive parameters as a representative. Consequently, in the absence of z dependence the internal virtual work expression (2.20) applies for both plane gradient elasticity models. Without loosing generality of our analysis, we assume that the stress, strain and displacement fields are independent of z coordinate and adopt (2.20) as our energy expression.

Remark 3. *If we had considered the theory of gradient elasticity in a plain manner as a constitutive relationship of the form* (2.8) *and replaced the classical stress tensor* (2.4) *in the classical internal virtual work expression by the gradient-elastic stress tensor* (2.8) *we would have written the internal energy in the form*

$$\delta W_{int} = t\int_\Omega (1 - g^2\Delta)\boldsymbol{\sigma} : \boldsymbol{\varepsilon}(\delta\boldsymbol{u})\,\mathrm{d}\Omega \tag{2.31}$$

which is an inconsistent expression. Namely, although this integral expression can be derived from (2.20) *by applying integration by parts, the set of corresponding boundary conditions would be inconsistent due to a missing boundary integral term. This will be shown explicitly in Section 3 dedicated to the governing equations and boundary conditions.*

Finally, with the assumed external loadings $\boldsymbol{f} = (f_x(x,y), f_y(x,y), 0)$ and $\boldsymbol{t} = \boldsymbol{0} = \boldsymbol{t}_l$, the external virtual work (2.9) can be written over the midsurface Ω simply as

$$\delta W_{\text{ext}}^{\text{c}} = \int_{\mathcal{P}} \boldsymbol{f} \cdot \delta \boldsymbol{u} \, \mathrm{d}\mathcal{P} = t \int_{\Omega} \boldsymbol{f} \cdot \delta \boldsymbol{u} \, \mathrm{d}\Omega. \tag{2.32}$$

3. Euler equations

In this section, the principle of virtual work, or virtual displacements, is taken as a starting point for obtaining the strong form of the problems, i.e., the governing equations with the corresponding sets of boundary and corner conditions, the latter ones often omitted in the literature. As can be seen already in one of the orginal works of Mindlin [36], the boundary conditions and their physical meaning are relevant and non-trivial issues for higher-order continuum models. In particular, we introduce here the additional attributes *singly* and *doubly* for different boundary conditions types.

3.1. Strong form for the static gradient elastic rod problem

The first step is to apply integration by parts in (2.14), (once) for the classical strain energy term and (twice) for the gradient term, and then to collect together the classical and non-classical parts:

$$\begin{aligned}
\delta W_{\text{int}} &= -\int_{\Omega} (A\,E\,\epsilon_{xx})' \,\delta u \,\mathrm{d}x + [A\,E\,\epsilon_{xx}\,\delta u]_{\Omega} + \int_{\Omega} (g^2 A\,(E\,\epsilon'_{xx}))'' \,\delta u \,\mathrm{d}x \\
&\quad - [(g^2 A\,(E\,\epsilon'_{xx}))'\,\delta u]_{\Omega} + [g^2 A\,(E\,\epsilon'_{xx})\,(\delta u)']_{\Omega} \\
&= -\int_{\Omega} \left((A\,E\,\epsilon_{xx})' - (g^2 A\,(E\,\epsilon'_{xx}))'' \right) \delta u \,\mathrm{d}x \\
&\quad + [\left(A\,E\,\epsilon_{xx} - (g^2 A\,(E\,\epsilon'_{xx}))'\right) \delta u]_{\Omega} + [g^2 A\,(E\,\epsilon'_{xx})\,(\delta u)']_{\Omega}.
\end{aligned} \tag{3.1}$$

Second, the energy balance of the internal virtual work and the external virtual work, $\delta W_{\text{ext}}^{\text{c}} + \delta W_{\text{ext}}^{\nabla} = \delta W_{\text{ext}} = \delta W_{\text{int}} = \delta W_{\text{int}}^{\text{c}} + \delta W_{\text{int}}^{\nabla}$, valid for all

kinematically admissible displacement variations δu, gives us the governing equation of the problem,

$$(A\,E\,\epsilon_{xx})' - (g^2 A\,E\,\epsilon'_{xx})'' + A\,f = 0 \quad \text{in } \Omega, \tag{3.2}$$

which can be written in terms of displacement for constant cross sections as

$$E\,A\,u'' - g^2 E\,A\,u'''' + A\,f = 0 \quad \text{in } \Omega. \tag{3.3}$$

The boundary conditions, both essential and natural ones, corresponding to (3.2) or (3.3) are implied by the energy balance in the following form:

$$u = \overline{u} \quad \text{or} \quad A\,E\,\epsilon_{xx} - (g^2 A\,E\,\epsilon'_{xx})' = A\overline{t}^g, \tag{3.4}$$

$$u' = \overline{w} \quad \text{or} \quad g^2 A\,E\,\epsilon'_{xx} = A\overline{d}^g \quad \text{on } \partial\Omega = \{0, L\}. \tag{3.5}$$

The overlined given boundary values, the displacement $\overline{u}$, and its conjugate quantity, the traction force $\overline{t}^g$ related to appropriate parts of $\boldsymbol{t}$ and $\boldsymbol{t}_l$ of (2.9)), are already present in the classical case with $g = 0$. Instead, the derivative of the displacement $\overline{w}$ and the double traction force $\overline{d}^g$ (related to appropriate parts of $\boldsymbol{r}$ of (2.9)) are the additional given boundary quantities provided by the gradient-elastic model.

From the physical point of view, the boundary conditions above should be now grouped such that they distinguish which type of the additional boundary conditions is applied. Let us give these two types additional attributes *singly* – refering to unprescribed derivative of the displacement – and *doubly* – refering to prescribed derivative – with the subscripts s and d, respectively. Altogether, four different boundary condition types can be defined: For *doubly clamped* and *singly clamped* boundaries (end points), $\Gamma_{\mathrm{C_d}}$ and $\Gamma_{\mathrm{C_s}}$, respectively,

$$u = \overline{u} \quad \text{and} \quad u' = \overline{w} \quad \text{on } \Gamma_{\mathrm{C_d}}, \tag{3.6}$$

$$u = \overline{u} \quad \text{and} \quad g^2 A\,E\epsilon'_{xx} = A\overline{d}^g \quad \text{on } \Gamma_{\mathrm{C_s}}, \tag{3.7}$$

whereas for *singly free* and *doubly free* boundaries, $\Gamma_{\mathrm{F_s}}$ and $\Gamma_{\mathrm{F_d}}$, respectively,

$$A\,E\epsilon_{xx} - (g^2 A\,E\epsilon'_{xx})' = A\overline{t}^g \quad \text{and} \quad u' = \overline{w} \quad \text{on } \Gamma_{\mathrm{F_s}}, \tag{3.8}$$

$$A\,E\epsilon_{xx} - (g^2 A\,E\epsilon'_{xx})' = A\overline{t}^g \quad \text{and} \quad g^2 A\,E\epsilon'_{xx} = A\overline{d}^g \quad \text{on } \Gamma_{\mathrm{F_d}}. \tag{3.9}$$

According to the boundary condition types above, the boundary of the domain is assumed to be composed of disjoint end point sets as $\partial\Omega = \Gamma_{\mathrm{C_d}} \cup \Gamma_{\mathrm{C_s}} \cup \Gamma_{\mathrm{F_d}} \cup \Gamma_{\mathrm{F_s}}$.

3.2. Strong form for the static plane gradient elasticity problems

As above for the bar problem, the first step is to apply integration by parts (once) for the classical strain energy, the first term in the energy expression (2.20) of the plane stress/strain problems. The second step is to apply integration by parts (twice) for the strain energy of the gradient-elastic augmentation. These steps are accomplished in detail in the Appendix. Finally, we use definition (2.8) and collect the classical and non-classical parts from (7.1), (7.4) and (7.5) together in order to apply the principle of the virtual work in (7.3) valid for all kinematically admissible variations $\delta\boldsymbol{u}$. However, let us first assume that the boundary is smooth, which allows us to neglect the corner jump terms implying that

$$\begin{aligned}\delta W_{\text{int}} = &-t\int_{\Omega}\mathbf{div}\,\boldsymbol{\sigma}^g\cdot\delta\boldsymbol{u}\,\mathrm{d}\Omega\\ &+t\int_{\partial\Omega}\Big(\boldsymbol{\sigma}^g\boldsymbol{n}-g^2\frac{\partial((\boldsymbol{\nabla}\boldsymbol{\sigma})\boldsymbol{n})\boldsymbol{s}}{\partial s}\Big)\cdot\delta\boldsymbol{u}\,\mathrm{d}s\\ &+g^2t\int_{\partial\Omega}\kappa(s)((\boldsymbol{\nabla}\boldsymbol{\sigma})\boldsymbol{n})\boldsymbol{n}\cdot\delta\boldsymbol{u}\,\mathrm{d}s\\ &+g^2t\int_{\partial\Omega}((\boldsymbol{\nabla}\boldsymbol{\sigma})\boldsymbol{n})\boldsymbol{n}\cdot((\boldsymbol{\nabla}(\delta\boldsymbol{u}))\boldsymbol{n}\,\mathrm{d}s,\end{aligned}\tag{3.10}$$

which gives us the governing equation of the problem based on the energy balance of the internal virtual work (3.10) and the external virtual work (2.32):

$$-\mathbf{div}\,\boldsymbol{\sigma}^g=\boldsymbol{f}\quad\text{in }\Omega,\tag{3.11}$$

which can be written, by (2.21) in terms of strains, or further in terms of displacements, as a a fourth-order partial differential equation of Lame type:

$$-(1-g^2\Delta)\big((\lambda+\mu)\nabla\mathrm{div}\,\boldsymbol{u}+\mu\Delta\boldsymbol{u}\big)=\boldsymbol{f}\quad\text{in }\Omega,\tag{3.12}$$

where ∇ denotes the standard vector-valued gradient operator.

The boundary conditions, both essential and natural ones, are implied by the energy balance in the following form:

$$\boldsymbol{u}=\overline{\boldsymbol{u}}\quad\text{or}\quad\boldsymbol{\sigma}^g\boldsymbol{n}-g^2\frac{\partial((\boldsymbol{\nabla}\boldsymbol{\sigma})\boldsymbol{n})\boldsymbol{s}}{\partial s}+\kappa(s)g^2((\boldsymbol{\nabla}\boldsymbol{\sigma})\boldsymbol{n})\boldsymbol{n}=\overline{\boldsymbol{t}}^g,\tag{3.13}$$

$$(\boldsymbol{\nabla}\boldsymbol{u})\boldsymbol{n}=\overline{\boldsymbol{w}}\quad\text{or}\quad g^2((\boldsymbol{\nabla}\boldsymbol{\sigma})\boldsymbol{n})\boldsymbol{n}=\overline{\boldsymbol{g}}^g\quad\text{on }\partial\Omega.\tag{3.14}$$

The overlined given boundary variables, the displacement $\overline{\boldsymbol{u}}$, and its conjugate quantity, the traction force $\overline{\boldsymbol{t}}^g$ (related to appropriate parts of $\boldsymbol{t}$ and $\boldsymbol{t}_l$ of (2.9)), are already present in the classical case with $g = 0$. Instead, the normal component of the displacement gradient $\overline{\boldsymbol{w}}$ and the double traction force $\overline{\boldsymbol{g}}^g$ (related to appropriate parts of $\boldsymbol{r}$ of (2.9)) are the additional given boundary quantities provided by the gradient-elastic model.

The boundary conditions above are now grouped in a similar way as for the bar problem above with the additional attribute *singly* now refering to unprescribed normal components of the displacement gradient and *doubly* refering to prescribed ones: For *doubly clamped* and *singly clamped* boundaries, respectively,

$$\boldsymbol{u} = \overline{\boldsymbol{u}} \quad \text{and} \quad (\boldsymbol{\nabla u})\boldsymbol{n} = \overline{\boldsymbol{w}} \quad \text{on } \Gamma_{\mathrm{C_d}}, \tag{3.15}$$

$$\boldsymbol{u} = \overline{\boldsymbol{u}} \quad \text{and} \quad g^2((\boldsymbol{\nabla\sigma})\boldsymbol{n})\boldsymbol{n} = \overline{\boldsymbol{g}}^g \quad \text{on } \Gamma_{\mathrm{C_s}}. \tag{3.16}$$

whereas for *singly free* and *doubly free* boundaries, respectively,

$$\boldsymbol{\sigma}^g\boldsymbol{n} - g^2\frac{\partial((\boldsymbol{\nabla\sigma})\boldsymbol{n})\boldsymbol{s}}{\partial s} + \kappa(s)g^2((\boldsymbol{\nabla\sigma})\boldsymbol{n})\boldsymbol{n} = \overline{\boldsymbol{t}}^g \quad \text{and} \tag{3.17}$$

$$(\boldsymbol{\nabla u})\boldsymbol{n} = \overline{\boldsymbol{w}} \quad \text{on } \Gamma_{\mathrm{F_s}}, \tag{3.18}$$

$$\boldsymbol{\sigma}^g\boldsymbol{n} - g^2\frac{\partial((\boldsymbol{\nabla\sigma})\boldsymbol{n})\boldsymbol{s}}{\partial s} + \kappa(s)g^2((\boldsymbol{\nabla\sigma})\boldsymbol{n})\boldsymbol{n} = \overline{\boldsymbol{t}}^g \quad \text{and} \tag{3.19}$$

$$g^2((\boldsymbol{\nabla\sigma})\boldsymbol{n})\boldsymbol{n} = \overline{\boldsymbol{g}}^g \quad \text{on } \Gamma_{\mathrm{F_d}}. \tag{3.20}$$

The boundary of the domain is assumed to be composed of disjoint open sets of boundary curves as $\partial\Omega = \Gamma_{\mathrm{C_d}} \cup \Gamma_{\mathrm{C_s}} \cup \Gamma_{\mathrm{F_d}} \cup \Gamma_{\mathrm{F_s}}$. In addition, one can still distinguish clamping the tangential and normal components of the vectors above.

The corner conditions of the problem follow from (7.5):

$$g^2\big(((\boldsymbol{\nabla\sigma})\boldsymbol{n}_m)\boldsymbol{s}_m - ((\boldsymbol{\nabla\sigma})\boldsymbol{n}_{m+1})\boldsymbol{s}_{m+1}\big) = \overline{\boldsymbol{t}_l}^g \quad \text{at } c_m \in \partial\Omega. \tag{3.21}$$

The overlined given traction force $\overline{\boldsymbol{t}_l}^g$ is related to appropriate parts of $\boldsymbol{t}_l$ present in (2.9).

3.3. Strong forms for vibration problems

For analysing vibrations, we here simply recall the corresponding governing equations [13]. For the bar model, the equation of motion is written as

$$EAu'' - g^2EAu'''' = \rho A\ddot{u} - \gamma^2\rho A\ddot{u}'', \tag{3.22}$$

with $\ddot{u}$ standing for the second time derivative of the displacement and γ denoting the new gradient parameter related to the micro-inertia. For the plane problem, in turn, it holds that

$$(1 - g^2\Delta)\big((\lambda + \mu)\nabla \mathrm{div}\, \boldsymbol{u} + \mu\Delta\boldsymbol{u}\big) = (1 - \gamma^2\Delta)\rho\ddot{\boldsymbol{u}}. \tag{3.23}$$

4. Variational formulations and solvability

In this section, the problems are formulated in variational forms within Sobolev space settings. Within this context, the solvability of the problem is proved by first proving the continuity and coercivity of the problems. In particular, these results provide a basis for many variational discretization methods such as Galerkin or Petrov–Galerkin methods.

In what follows, we will use the notation $H^s(\Omega)$ for a real Sobolev space of order s consisting of square integrable real-valued functions defined on Ω with square integrable weak derivatives up to order s. The corresponding Sobolev norm is denoted by $||\cdot||_s$ and the seminorm by $|\cdot|_s$.

4.1. Weak form for the gradient elastic rod problem

In this section, we assume that energy expressions (2.14) and (2.16), are scaled by $D = EA$ such that $\hat{f} = f/E$, with EA assumed to be constant. This implies a dimensionless formulation with L as the length unit. For clarity, the hat notation is omitted in the formulations below, however. For simplicity, g is assumed to be constant as well.

The variational formulation of the gradient-elastic bar problem corresponding to (2.14) and (2.16) reads as follows:

Problem 1. *For $f \in L^2(\Omega)$, find $u \in U \subset H^2(\Omega)$ such that*

$$a(u, v) = l(v) \quad \forall v \in V \subset H^2(\Omega), \tag{4.1}$$

where the bilinear form $a : U \times V \to \mathbb{R}$, $a(u, v) = a^c(u, v) + a^\nabla(u, v)$, and the load functional $l : V \to \mathbb{R}$, respectively, are defined as

$$a^c(u, v) = \int_0^L u'\, v'\, \mathrm{d}x, \quad a^\nabla(u, v) = \int_0^L g^2 u''v''\, \mathrm{d}x, \quad l(v) = \int_0^L f\, v\, \mathrm{d}x. \tag{4.2}$$

The trial function set

$$U = \{v \in H^2(\Omega) \ \mid \ u_{|\Gamma_{C_d} \cup \Gamma_{C_s}} = \bar{u}, \ u'_{|\Gamma_{C_d} \cup \Gamma_{F_s}} = \bar{w}\} \tag{4.3}$$

consists of functions satisfying the essential boundary conditions, with the given Dirichlet data $\bar{u}, \bar{w}$, while the test function space V consists of H^2 functions satisfying the corresponding homogeneous Dirichlet boundary conditions.

The energy norm of the problem induced by the bilinear form, defined as

$$\|v\|_a^2 = |v|_1^2 + g^2 |v|_2^2,$$

is equivalent to the H^2 norm whenever $U = V$, which can be seen in the proofs of the theorems. In addition, the symmetry of the bilinear form is clearly guaranteed: $a(u, v) = a(v, u)\ \forall u, v \in V$. In the limit case $g = 0$, the bilinear form of the problem reduces to the classical one requiring only H^1 regular functions.

The continuity and coercivity of the bilinear form – for each positive g – guarantees the well-posedness of the problem. The proofs of the theorems are given in Appendix. For simplicity, the proofs are provided here for singly clamped bars with $\partial\Omega = \Gamma_{C_s}$ and $U = V$.

Theorem 1. *Let us assume that $\partial\Omega = \Gamma_{C_s}$ and $U = V$. For any g, there exists a positive constant $C_1 = C_1(g)$ such that*

$$a(u, v) \leq C_1 \|u\|_2 \|v\|_2 \quad \forall u, v \in V. \tag{4.4}$$

Theorem 2. *Let us assume that $\partial\Omega = \Gamma_{C_s}$ and $U = V$. For any $g > 0$, there exists a positive constant $\alpha_1 = \alpha_1(g)$ such that*

$$a(v, v) \geq \alpha_1 \|v\|_2^2 \quad \forall v \in V. \tag{4.5}$$

It should be noticed that the coercivity constant α_1 which will be present in the error estimates of the numerical method proposed in Section 5 is clearly dependent on the gradient parameter g. This issue will be studied numerically in Section 6.

Finally, according to Riesz Representation Theorem, the gradient-elastic rod problem with clamped boundaries has a unique solution:

Theorem 3. *Let us assume that $\partial\Omega = \Gamma_{C_s}$, $U = V$ and $g > 0$. For a given loading $f \in L^2(\Omega)$, Problem 1 has a unique solution in V.*

4.2. Weak form for the plane gradient elasticity problem

In this section, we assume that the thickness is divided from the energy expressions (2.20) and (2.32), and both $\boldsymbol{f}$ and $\boldsymbol{E}$ are scaled by $D = Et/(1-\nu^2)$ such that $\hat{\boldsymbol{f}} = t\boldsymbol{f}/D$ and $\hat{\boldsymbol{E}} = \boldsymbol{E}/D$. This implies a dimensionless formulation with $\operatorname{diam}(\Omega)$ as the length unit. For clarity, the hat notation is omitted in the formulations below, however.

The variational formulation of the plane gradient elasticity problem corresponding to (2.20) and (2.32), with (2.3) and (2.4), reads as follows:

Problem 2. *For $\boldsymbol{f} \in [L^2(\Omega)]^2$, find $\boldsymbol{u} \in \boldsymbol{U} \subset [H^2(\Omega)]^2$ such that*

$$a(\boldsymbol{u}, \boldsymbol{v}) = l(\boldsymbol{v}) \quad \forall \boldsymbol{v} \in \boldsymbol{V} \subset [H^2(\Omega)]^2, \tag{4.6}$$

where the bilinear form $a : \boldsymbol{U} \times \boldsymbol{V} \to \mathbb{R}$, $a(\boldsymbol{u}, \boldsymbol{v}) = a^c(\boldsymbol{u}, \boldsymbol{v}) + a^\nabla(\boldsymbol{u}, \boldsymbol{v})$, and the load functional $l : \boldsymbol{V} \to \mathbb{R}$ are, respectively, defined as

$$a^c(\boldsymbol{u}, \boldsymbol{v}) = \int_\Omega \boldsymbol{E}\boldsymbol{\varepsilon}(\boldsymbol{u}) : \boldsymbol{\varepsilon}(\boldsymbol{v}) \,\mathrm{d}\Omega, \tag{4.7}$$

$$a^\nabla(\boldsymbol{u}, \boldsymbol{v}) = \int_\Omega g^2 \boldsymbol{\nabla}(\boldsymbol{E}\boldsymbol{\varepsilon}(\boldsymbol{u})) \vdots \boldsymbol{\nabla}\boldsymbol{\varepsilon}(\boldsymbol{v}) \,\mathrm{d}\Omega, \tag{4.8}$$

$$l(\boldsymbol{v}) = \int_\Omega \boldsymbol{f} \cdot \boldsymbol{v} \,\mathrm{d}\Omega. \tag{4.9}$$

The trial function set

$$\boldsymbol{U} = \{\boldsymbol{v} \in [H^2(\Omega)]^2 \;\mid\; \boldsymbol{v}_{|\Gamma_{\mathrm{C_s}} \cup \Gamma_{\mathrm{C_d}}} = \overline{\boldsymbol{u}},\ (\boldsymbol{\nabla}\boldsymbol{v})\boldsymbol{n}_{|\Gamma_{\mathrm{C_d}} \cup \Gamma_{\mathrm{F_s}}} = \overline{\boldsymbol{w}}\} \tag{4.10}$$

consists of functions satisfying the essential boundary conditions, with the given Dirichlet data $\overline{\boldsymbol{u}}$ and $\overline{\boldsymbol{w}}$, while the test function space $\boldsymbol{V}$ consists of $[H^2]^2$ functions satisfying the corresponding homogeneous Dirichlet boundary conditions.

The energy norm of the problem induced by the bilinear form, defined as

$$\begin{aligned} \|\boldsymbol{v}\|_a^2 = &\int_\Omega \big((1-\nu)\boldsymbol{\varepsilon}(\nabla v) + \nu \operatorname{tr}\boldsymbol{\varepsilon}(\nabla v)\boldsymbol{I}\big) : \boldsymbol{\varepsilon}(\nabla v) \,\mathrm{d}\Omega \\ &+ \int_\Omega g^2 \big((1-\nu)\boldsymbol{\nabla}\boldsymbol{\varepsilon}(\nabla v) + \nu\, \boldsymbol{\nabla}(\operatorname{tr}\boldsymbol{\varepsilon}(\nabla v)\boldsymbol{I})\big) \vdots \boldsymbol{\nabla}\boldsymbol{\varepsilon}(\nabla v) \,\mathrm{d}\Omega, \end{aligned} \tag{4.11}$$

is equivalent to the H^2 norm whenever $\boldsymbol{U} = \boldsymbol{V}$, which can be seen in the proofs of the theorems given in Appendix. In addition, the symmetry of the

bilinear form is clearly guaranteed: $a(\boldsymbol{u},\boldsymbol{v}) = a(\boldsymbol{v},\boldsymbol{u}) \forall \boldsymbol{u},\boldsymbol{v} \in \boldsymbol{V}$. In the limit case $g = 0$, the bilinear form of the problem reduces to the classical case of H^1 functions.

The continuity and coercivity of the bilinear form – for each positive g – guarantees the well-posedness of the problem. For simplicity, the proof is provided here for clamped boundaries.

Theorem 4. *Let us assume that $\partial\Omega = \Gamma_{C_s}$ and $\boldsymbol{U} = \boldsymbol{V}$. For any g, there exists a positive constant $C_2 = C_2(g)$ such that*

$$a(\boldsymbol{u},\boldsymbol{v}) \leq C_2 \|\boldsymbol{u}\|_2 \|\boldsymbol{\varphi}\|_2 \quad \forall \boldsymbol{u},\boldsymbol{v} \in \boldsymbol{V}. \tag{4.12}$$

Theorem 5. *Let us assume that Ω is convex with a Lipschitz-continuous boundary $\partial\Omega = \Gamma_{C_s}$, and $\boldsymbol{U} = \boldsymbol{V}$. For any $g > 0$ and $\nu < 1$, there exists a positive constant $\alpha_2 = \alpha_2(g)$ such that*

$$a(\boldsymbol{v},\boldsymbol{v}) \geq \alpha_2 \|\boldsymbol{v}\|_2^2 \quad \forall \boldsymbol{v} \in \boldsymbol{V}. \tag{4.13}$$

In this case, there is a a clear dependence on the Poisson ratio in the coercivity constant α_2, as in the classical elasticity. In addition, the coercivity constant depends on the gradient parameter g. The effect of this dependence on the error estimates of the numerical method proposed in Section 5 will be studied numerically in Section 6.

Finally, according to Riesz Representation Theorem, the plane gradient elasticity problem with clamped boundaries has a unique solution:

Theorem 6. *Let us assume that Ω is convex with a Lipschitz-continuous boundary $\partial\Omega = \Gamma_{C_s}$, $\boldsymbol{U} = \boldsymbol{V}$, $g > 0$ and $\nu < 1$. For a given loading $\boldsymbol{f} \in [L^2(\Omega)]^2$, Problem 2 has a unique solution in $\boldsymbol{V}$.*

Remark 4. *For Mindlin's Form II model, the non-classical part of the bilinear form of Problem 2 would be defined as (see Remark 1)*

$$a^{\nabla}(\boldsymbol{u},\boldsymbol{v}) = \int_{\Omega} \boldsymbol{G}\boldsymbol{\nabla}\boldsymbol{\varepsilon}(\boldsymbol{u}) \vdots \boldsymbol{\nabla}\boldsymbol{\varepsilon}(\boldsymbol{v}) \, \mathrm{d}\Omega. \tag{4.14}$$

This more general form would complicate the corresponding proofs of continuity and coercivity (see the Appendix), and, accordingly, imply some conditions for the involved five gradient parameters through the positive-definity requirements for $\boldsymbol{G}$, especially.

5. Isogeometric Galerkin methods

In this section, we first briefly recall the the isogeometric tensor product discretizations which are then applied for solving Problems 1 and 2 by conforming Galerkin methods with corresponding error estimates to be confirmed in Section 6.

5.1. Basics of the isogeometric approaches

Let us use the plane problem as an example since the one-dimensional setting for the bar problem follows as a special case (see [14, 43, 18], for instance).

First, we introduce an isoparametric discrete space for the approximation of the displacement field such that $\boldsymbol{u}_h \in [S_h]^2$ with

$$S_h = \{R_{i,j}^{p,q} \circ \boldsymbol{F}^{-1}\}. \tag{5.1}$$

The geometrical mapping between the two-dimensional parametric space $[0,1] \times [0,1]$ and the midsurface $\bar{\Omega}$ is defined by $\boldsymbol{F} : [0,1] \times [0,1] \to \bar{\Omega}$ as

$$\boldsymbol{F}(\xi,\eta) = \sum_{i=1}^{n}\sum_{j=1}^{m} R_{i,j}^{p,q}(\xi,\eta)\boldsymbol{B}_{i,j} \tag{5.2}$$

providing an isogeometric NURBS discretization. Above, $\boldsymbol{B}_{i,j}$, $i = 1 \dots n, j = 1 \dots m$, denote the control points, while the NURBS basis functions are defined as

$$R_{i,j}^{p,q}(\xi,\eta) = \frac{N_{i,p}(\xi)M_{j,q}(\eta)w_{i,j}}{\sum_{\hat{i}=1}^{n}\sum_{\hat{j}=1}^{m} N_{\hat{i},p}(\xi)M_{\hat{j},q}(\eta)w_{\hat{i},\hat{j}}} \tag{5.3}$$

The B-spline basis functions $N_{i,p}$ and $M_{j,q}$ of order p and q, respectively, associated to the open knot vectors (allowing knot repetitions) $\{0 = \xi_1, \dots, \xi_{n+p+1} = 1\}$ and $\{0 = \eta_1, \dots, \eta_{m+q+1} = 1\}$, respectively, are defined on the basis of the Cox–de Boor recursion:

$$N_{i,0}(\xi) = \begin{cases} 1, & \xi_i \le \xi < \xi_{i+1}, \\ 0, & \text{otherwise} \end{cases} \tag{5.4}$$

$$N_{i,p}(\xi) = \frac{\xi - \xi_i}{\xi_{i+p} - \xi_i} N_{i,p-1}(\xi) + \frac{\xi_{i+p+1} - \xi}{\xi_{i+p+1} - \xi_{i+1}} N_{i+1,p-1}(\xi). \tag{5.5}$$

The associated tensor product mesh of the midsurface is defined as

$$\mathcal{T}_h = \{K = \boldsymbol{F}((\xi_i, \xi_{i+1}) \times (\eta_j, \eta_{j+1})) \mid 1 \leq i \leq m_p - 1, 1 \leq j \leq m_q - 1\}, \tag{5.6}$$

with m_p and m_q referring to the number of knots without repetitions (see [43, 20], for instance, for more details) with the mesh size $h = \max_{K \in \mathcal{T}_h} h_K$ (serving as the mesh index, as usual) defined by the element size $h_K = \mathrm{diam}(K)$.

Finally, by assuming $p = q$ and global regularity C^{p-1} over $\mathcal{T}_h$, with $p \geq 2$, it holds that $S_h \subset H^2(\Omega)$, which provides a conforming and consistent Galerkin method allowing the formulation of Method 2 with $\boldsymbol{U}_h = [S_h]^2 \cap \boldsymbol{U}$, $\boldsymbol{V}_h = [S_h]^2 \cap \boldsymbol{V}$.

5.2. Discrete formulations and error estimates

Let us solve Problems 1 and 2, respectively, by conforming isogeometric Galerkin methods formulated as follows:

Method 1. *For $f \in L^2(\Omega)$, find $u_h \in U_h \subset U$ such that*

$$a(u_h, v) = l(v) \quad \forall v \in V_h \subset V. \tag{5.7}$$

Method 2. *For $\boldsymbol{f} \in [L^2(\Omega)]^2$, find $\boldsymbol{u}_h \in \boldsymbol{U}_h$ such that*

$$a(\boldsymbol{u}_h, \boldsymbol{v}) = l(\boldsymbol{v}) \quad \forall \boldsymbol{v} \in \boldsymbol{V}_h \subset \boldsymbol{V}. \tag{5.8}$$

For doubly clamped and singly free boundary conditions, i.e., for U and $\boldsymbol{U}$ with $\Gamma_{\mathrm{C_d}} \cup \Gamma_{\mathrm{F_s}} \neq \emptyset$ meaning fixed displacement derivatives, we propose excluding the corresponding essential boundary conditions from the function spaces and using weak enforcement instead, with an accordingly augmented bilinear form: either the so called Nitsche's method which can be shown to provide a consistent, symmetric and stable bilinear form (see [44, 45, 46, 18], for instance), Lagrange multipliers, or simply the classical symmetrized penalization method.

With the conformity of the methods, the continuity and coercivity of the continuous problems are inherited by the discrete methods implying error estimates which can be proved in a standard way by imitating the steps for proving Cea's lemma [39]:

Proposition 1. *Let us assume that* $\partial\Omega = \Gamma_{C_s}$, $U = V$ *and* $g > 0$. *For a given loading* $f \in L^2(\Omega)$, *it holds that*

$$\|u - u_h\|_2 \leq \frac{C_1}{\alpha_1} \inf_{0 \neq v \in V_h} \|u - v\|_2. \tag{5.9}$$

Proposition 2. *Let us assume that* Ω *is convex with a Lipschitz-continuous boundary* $\partial\Omega = \Gamma_{C_s}$, $\boldsymbol{U} = \boldsymbol{V}$, $g > 0$ *and* $\nu < 1$. *For a given loading* $\boldsymbol{f} \in [L^2(\Omega)]^2$, *it holds that*

$$\|\boldsymbol{u} - \boldsymbol{u}_h\|_2 \leq \frac{C_2}{\alpha_2} \inf_{\boldsymbol{0} \neq \boldsymbol{v} \in \boldsymbol{V}_h} \|\boldsymbol{u} - \boldsymbol{v}\|_2 \tag{5.10}$$

These qualitative error estimates give, with C^1-continuous discretizations, more quantitative estimates for the error by utilizing the approximation properties of NURBS functions [47, 43, 48] (as the corresponding classical ones for polynomes [49]):

Corollary 1. *With the assumptions of Proposition 1 the following error estimate holds and for the bar problem:*

$$\|u - u_h\|_2 \leq \frac{C_1}{\alpha_1} c h^{p-1} |u|_{p+1}. \tag{5.11}$$

where c denotes an interpolation constant and the exact solutions of the problems are assumed to be smooth enough, i.e., $u \in H^{p+1}(\Omega)$.

Corollary 2. *With the assumptions of Proposition 2, the following error estimate holds for the plane strain/stress problem:*

$$\|\boldsymbol{u} - \boldsymbol{u}_h\|_2 \leq \frac{C_2}{\alpha_2} c h^{p-1} |\boldsymbol{u}|_{p+1}, \tag{5.12}$$

where c denotes an interpolation constant and the exact solution of the problem is assumed to be smooth enough, i.e., $\boldsymbol{u} \in [H^{p+1}(\Omega)]^2$.

Numerical results in Section 6 with isogeometric methods of C^{p-1}-continuous NURBS basis functions of order $p \geq 2$ confirm these theoretical results providing the convergence order $\mathcal{O}(h^{p-1})$. For lower order norms, additional powers of h are obtained.

Remark 5. *Regarding the uniformity of these estimates with respect to the gradient parameter, one should notice that due to the fact that the coercivity constants α_i depend on g the error estimates are dependent on g as well. However, according to the numerical results in Section 6 the methods give good convergence results for a wide range of parameter values.*

Remark 6. *Regarding the regularity of the exact solution, one should notice that theses problems possess boundary layers depending on the gradient parameter g as can be seen in the benchmark solutions of Section 6. This stems from the fact that the number of boundary conditions jumps from two to one when the length scale parameter approaches zero. Refined error analysis, in the spirit of [50] for instance, is devoted to another contribution, however.*

6. Numerical results

In this section, we confirm the theoretical results by studying numerical benchmark problems and illustrating the differences between the models of classical and gradient elasticity.

Methods 1 and 2 have been implemented by applying the isogeometric approach [14] in three different environments: as an in-house academic Matlab code; as a part of the open source Matlab package GeoPDEs [51]; as user elements of the commercial FEM software Abaqus [52], described in [53]. The majority of the results presented here come from the (unreleased) GeoPDEs contributions but most of the results have been double-checked by the other implementations. The last example focusing on free in-plane vibrations of an annular plate have been analyzed by using the Abaqus user elements alone.

We notice that in the numerical results $g = 0 = \gamma$ refers to the solution following the classical elasticity theory.

6.1. Benchmarks for the static bar problem

Let us first consider a bar with singly clamped ends subject to an exponential distributed loading

$$f = \frac{f_0}{A} e^{x/L}. \tag{6.1}$$

The exact analytical solution of the problem is of the form

$$u(x) = c_1 e^{x/g} + c_2 e^{-x/g} + c_3 x + c_4 + \hat{u}(x), \tag{6.2}$$

where $\hat{u} = \hat{c}e^{x/L}$ denotes the particular solution depending on the loading (6.1) with

$$\hat{c} = -\frac{f_0 L^2}{EA(1 - g^2/L^2)}. \tag{6.3}$$

The constants $c_i, i = 1, ..., 4$ are determined by the boundary conditions giving

$$c_1 = -\hat{c}\frac{g^2(e - e^{-L/g})}{2L^2 \sinh(L/g)}, c_2 = -\hat{c}\frac{g^2(e^{L/g} - e)}{2L^2 \sinh(L/g)}, c_3 = \frac{f_0 L(e-1)}{EA}, c_4 = \frac{f_0 L^2}{EA}. \tag{6.4}$$

In the computations, we have used the following material data: $E = 200000$ MPa, $A = 1$ mm^2, $L = 10$ mm, $f_0 = 10000$ N/m, whereas for g different values have been adopted.

The first numerical tests are accomplished with $g/L = 0.05$. Fig. 1 shows that the convergence rates of the relative error in the H^2 norm is $\mathcal{O}(h^{p-1})$ for $p = 2, 3, 4, 5$ and hence in a very good agreement with the theoretical results of Corollary 1. The convergence rates for the H^1 and L^2 errors are depicted in Figs. 2 and 3 showing the corresponding improvements in the orders.

Convergence results in the H^2, H^1 and L^2 norms with $p = 3$ for two different values of the gradient parameter $g/L = 0.05$ and $g/L = 0.5$ are compared in Fig. 4. The value of the gradient-elastic modulus does not affect the asymptotic convergence rate although the error level is higher for the smaller gradient parameter value.

Let us next consider a cantilever bar without a body load ($f = 0$); the fixed end at $x = 0$ is singly clamped, $u(0) = 0$, whereas the other end is doubly free with an extensional applied force $P = 10000$ N:

$$A\,E\epsilon_{xx} - (g^2 A\,E\epsilon'_{xx})' = P \quad \text{and} \quad g^2 A\,E\epsilon'_{xx} = 0 \quad \text{at } x = L. \tag{6.5}$$

The exact solution of the problem is then of the form

$$u(x) = \frac{P}{E\,A}\Big(x - g\frac{\sinh(x/g)}{\cosh(L/g)}\Big). \tag{6.6}$$

In Fig. 5, the numerical solution is compared to the exact solution with two different mesh sizes (8 and 64 degrees of freedom with $p = 3$) and the non-classical part of the exact solution, i.e., the ratio of the hyperbolic sinus and cosine functions, is plotted in order to give an example of the boundary layer term present in the solution.

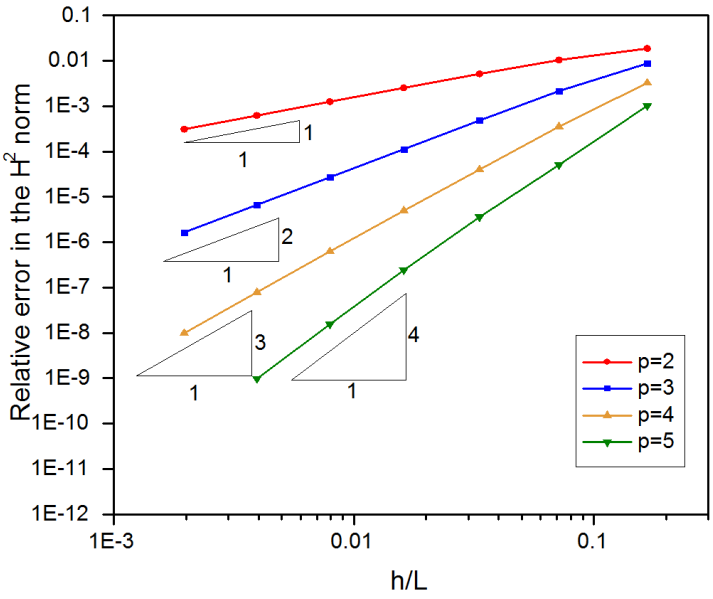

Figure 1: Clamped bar: Convergence in the H^2 norm for $p = 2, 3, 4, 5$ with $g/L = 0.05$.

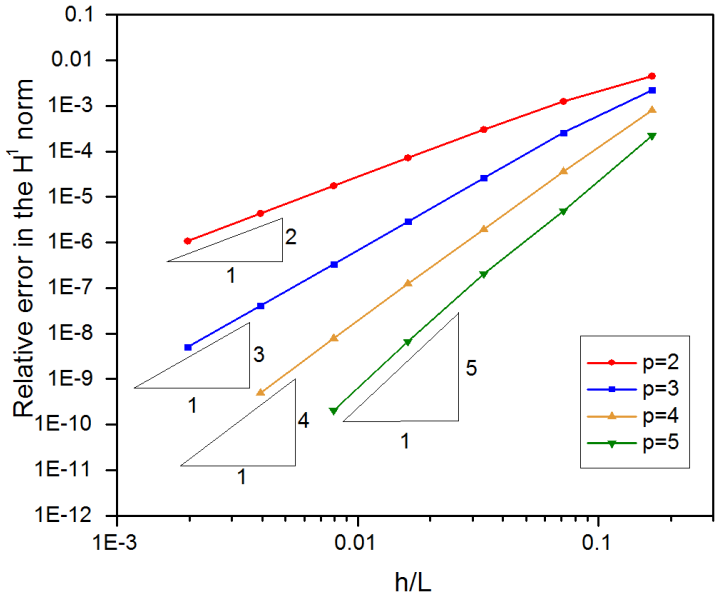

Figure 2: Singly clamped bar: Convergence in the H^1 norm for $p = 2, 3, 4, 5$ with $g/L = 0.05$.

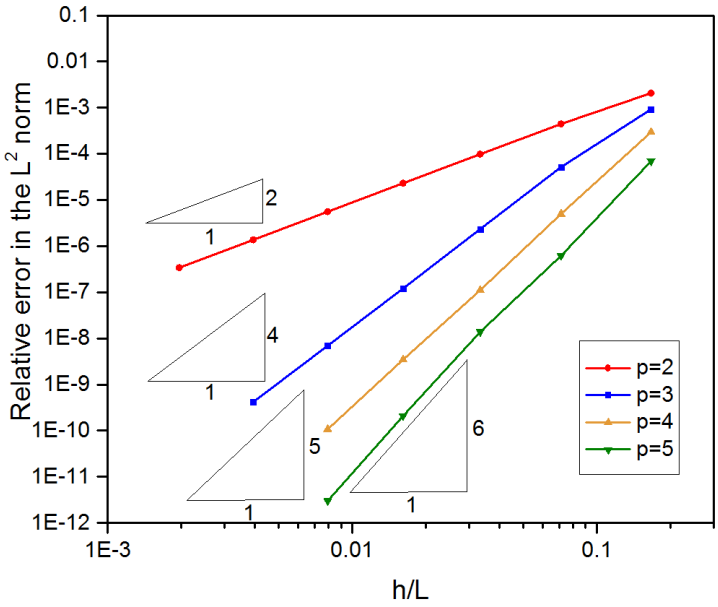

Figure 3: Singly clamped bar: Convergence in the L^2 norm for $p = 2, 3, 4, 5$ with $g/L = 0.05$.

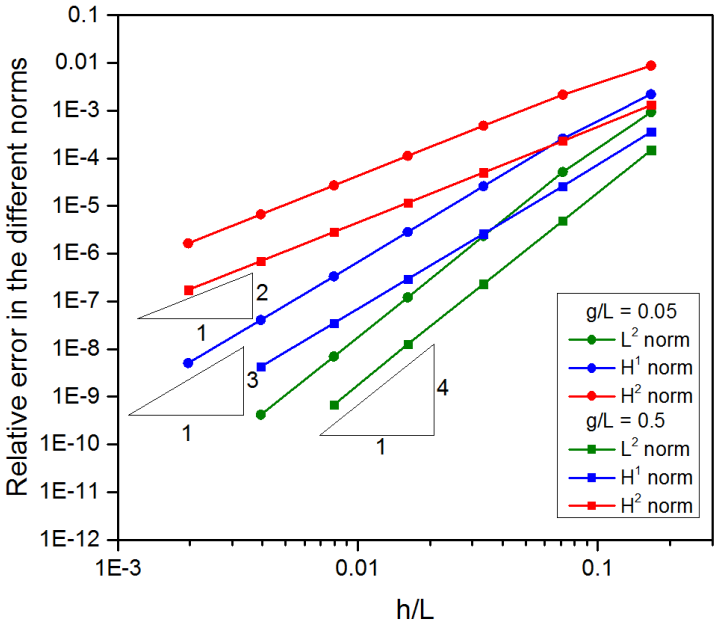

Figure 4: Singly clamped bar: Convergence in the H^2, H^1 and L^2 norms for $p = 3$ with $g/L = 0.05$ and $g/L = 0.5$.

The numerical solution obtained for the relative displacement and strain distributions, for $p = 3$ and 128 degrees of freedom, are depicted in Figs. 6 and 7 for different gradient parameters. They are in agreement with the analytical results in [24, 12].

For studying parameter dependence of the convergence rate, relative errors in the H^2 norm are now compared for eight different values of the gradient parameter g in Fig. 8. According to these curves, gradient-elastic modulus g does not affect the asymptotic convergence rate within the current mesh density range, although for small parameter values convergence is very slow for the coarse meshes which are not able to capture the layer of the solution. In addition, the error level is clearly affected by the gradient parameter: as g decreases, the error level increases.

6.2. A benchmark for extensional bar vibrations

For benchmarking wave propagation in gradient-elastic rods, let us consider a singly clamped bar and assume that the wave propagation is of the form

$$u(x,t) = u_0 e^{kx - i\omega t}. \tag{6.7}$$

After substituting (6.7) into (3.22) and applying the boundary conditions, one can determine wave number $k = \pi n/L$, with n denoting natural numbers, and the angular frequency

$$\omega = k\sqrt{\frac{E}{\rho}}\sqrt{\frac{1+g^2k^2}{1+\gamma^2k^2}}. \tag{6.8}$$

The wave amplitude u_0 depends on the initial condition and does not need to be determined here.

By using the analytical solution (6.8), one can obtain the normalised discrete spectra of Fig. 9 where $g/L = 0.1, \gamma/L = 0.1$ with 128 degrees of freedom for different orders of basis functions ($p = 2, 3, 4, 5$). The qualitative shapes of these curves coincide with the ones obtained by isogeometric analysis for the classical elasticity (cf. [54], for instance).

As can be seen in Figs. 10–12 for $p = 2, 3, 4$, changes in the gradient elasticity parameters g and γ affect the accuracy of the approximate spectra: increasing g increases the gap between analytical and numerical results, while increasing γ, in opposite, decreases the gap. In other words, for $g = 0.001 = \gamma$ (solid green line) the accuracy level is fairly close to the level of the classical

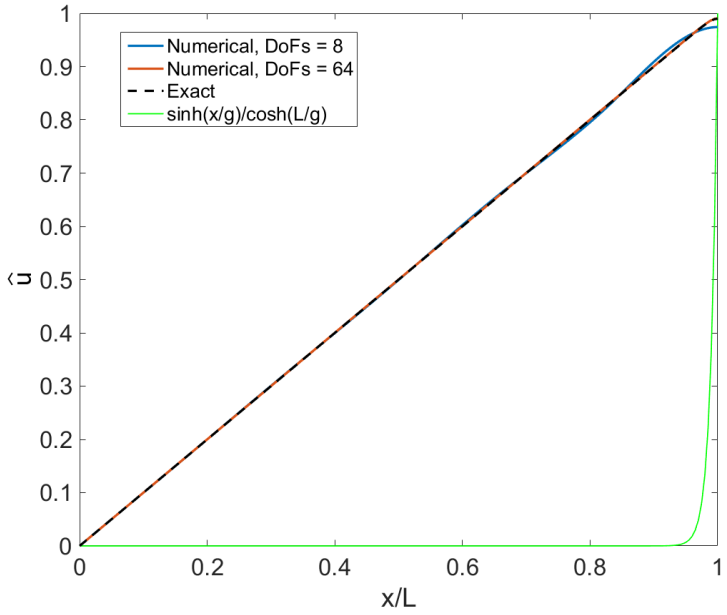

Figure 5: Singly clamped cantilever bar: Numerical and exact solutions and the gradient term $\sinh(x/g)/\cosh(L/g)$ for $g/L = 0.01$ with $p = 3$.

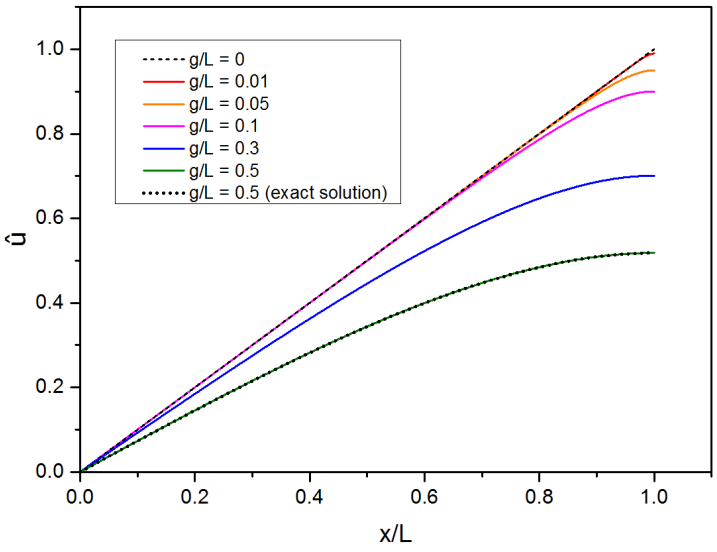

Figure 6: Singly clamped cantilever bar: Relative axial displacement $\hat{u} = u/u_c(L)$, with c refering to the classical solution, versus its dimensionless length for $g/L = 0, ..., 0.5$ with $p = 3$ and 128 degrees of freedom.

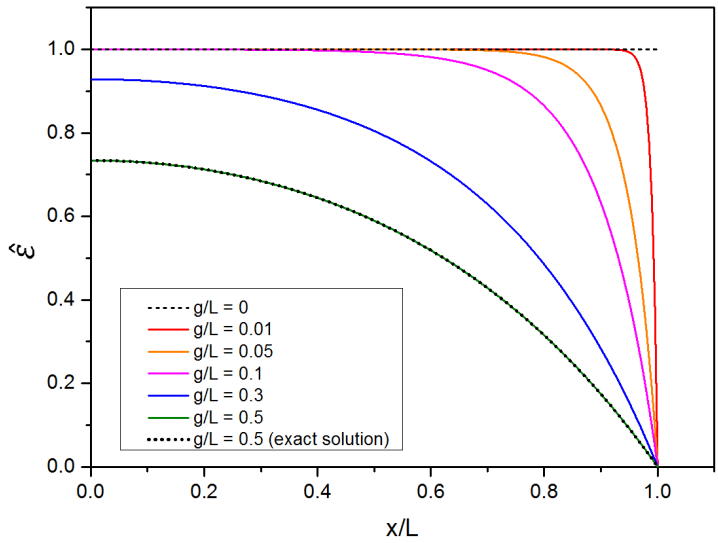

Figure 7: Singly clamped cantilever bar: Relative axial strain $\hat{\epsilon} = \epsilon/\epsilon_c(L)$, with c refering to the classical solution, versus its dimensionless length for $g/L = 0, ..., 0.5$ with $p = 3$ and 128 degrees of freedom.

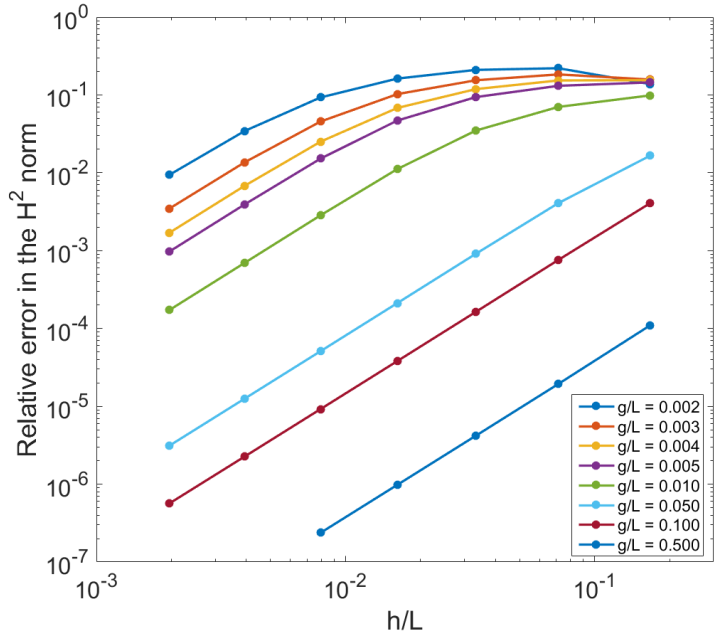

Figure 8: Singly clamped cantilever bar: Convergence in the H^2 norm for $p = 3$ with $g/L = 0.002, ..., 0.5$.

case $g = 0 = \gamma$ (black dashed line), whereas for $g/\gamma > 1$ (solid orange line) the accuracy clearly decreases and for $g/\gamma < 1$ (solid magenta line) the accuracy increases (cf. the ratio g/γ appearing in (6.9) and its limit $k \to \infty$).

Next, in Figs. 13–15, the convergence of the relative error in the H^2, H^1 and L^2 norms for $p = 2$ are presented for the fifth eigenmode of the problem. The convergence rates very accurately follow the orders $\mathcal{O}(h^{p-1}), \mathcal{O}(h^p)$ and $\mathcal{O}(h^{p+1})$, respectively.

Finally, in Fig. 16, the phase velocity

$$v^{g,\gamma} = \frac{\omega}{k} = \sqrt{\frac{E}{\rho}}\sqrt{\frac{1+g^2k^2}{1+\gamma^2k^2}} = v^{0,0}\sqrt{\frac{1+g^2k^2}{1+\gamma^2k^2}} \tag{6.9}$$

is reported for different values of gradient parameters for $p = 3$ and 128 degrees of freedom. In particular, it should be noticed that $v^{g,\gamma} \to v^{0,0}g/\gamma$ for $k \to \infty$ for all $\gamma \neq 0$ giving a finite value for the limit. Instead, $v^{g,\gamma}$ tends to infinity without the gradient inertia term, i.e, with $\gamma = 0$ which justifies adopting the micro-inertia term (cf. [13]).

6.3. A benchmark for the static plane strain/stress problem

Let us consider a square plate $\Omega = (0, L) \times (0, L) \subset \mathbb{R}^2$ with a volume force field $\boldsymbol{f} = (f_x, f_y)$ given by

$$\begin{aligned} f_x(x,y) = 4\frac{\pi^2}{L^2}\sin(2\pi\frac{x}{L})\Big((2\mu+\lambda)(1+4\pi^2\frac{g^2}{L^2}) \\ - 2\mu\cos(2\pi\frac{y}{L})(1+8\pi^2\frac{g^2}{L^2})\Big), \end{aligned} \tag{6.10}$$

$$\begin{aligned} f_y(x,y) = 4\frac{\pi^2}{L^2}\sin(2\pi\frac{y}{L})\Big(-(2\mu+\lambda)(1+4\pi^2\frac{g^2}{L^2}) \\ + 2\mu\cos(2\pi\frac{x}{L})(1+8\pi^2\frac{g^2}{L^2})\Big), \end{aligned} \tag{6.11}$$

where μ and λ denote the material parameters of the plane stress state (which can be easily transformed to the plane strain case). The boundary of the plate is singly clamped as defined in (3.16). The analytical solution of the problem is of the form $\boldsymbol{u} = (u_x, u_y)$ with

$$u_x(x,y) = \sin(2\pi\frac{x}{L})(1-\cos(2\pi\frac{y}{L})), \tag{6.12}$$

$$u_y(x,y) = \sin(2\pi\frac{y}{L})(-1+\cos(2\pi\frac{x}{L})). \tag{6.13}$$

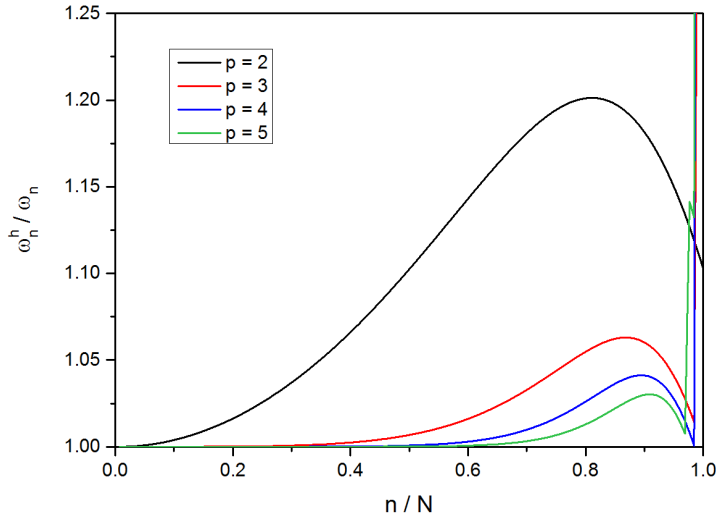

Figure 9: Singly clamped bar: Normalized discrete spectra for NURBS basis functions of orders $p = 2, 3, 4, 5$ with 128 degrees of freedom with $g/L = 0.1, \gamma/L = 0.1$.

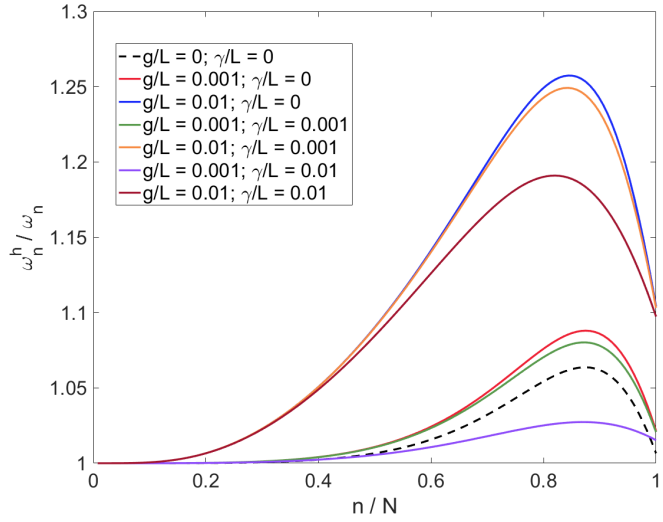

Figure 10: Singly clamped bar: Normalized discrete spectra for different pairs of g and γ with $p = 2$.

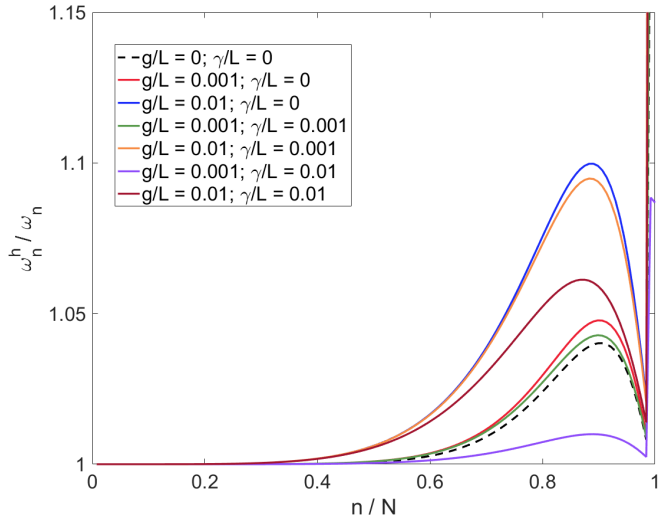

Figure 11: Singly clamped bar: Normalized discrete spectra for different pairs of g and γ with $p = 3$.

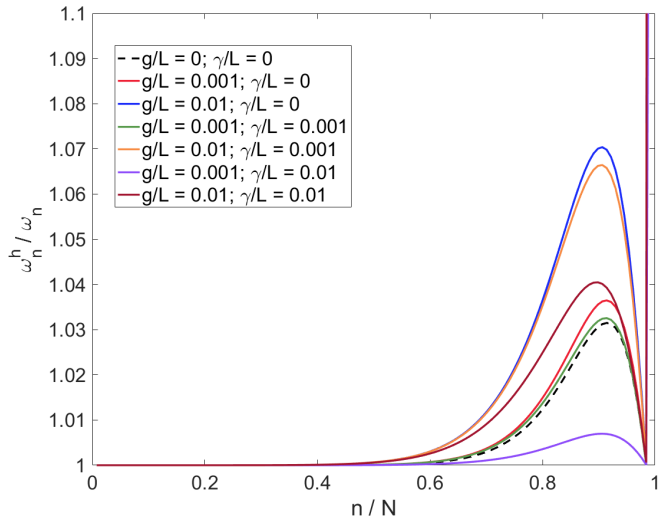

Figure 12: Singly clamped bar: Normalized discrete spectra for different pairs of g and γ with $p = 4$.

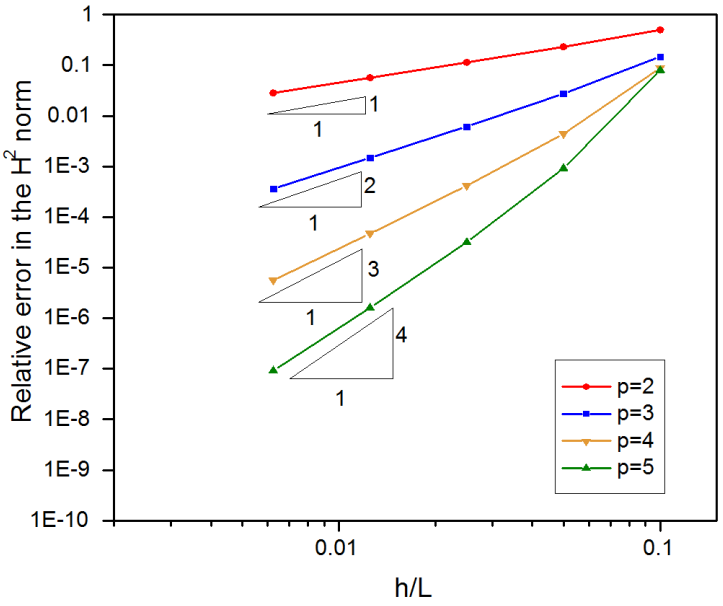

Figure 13: Singly clamped bar: Convergence of the fifth eigenmode in the H^2 norm with $g/L = 0.1, \gamma/L = 0.1$.

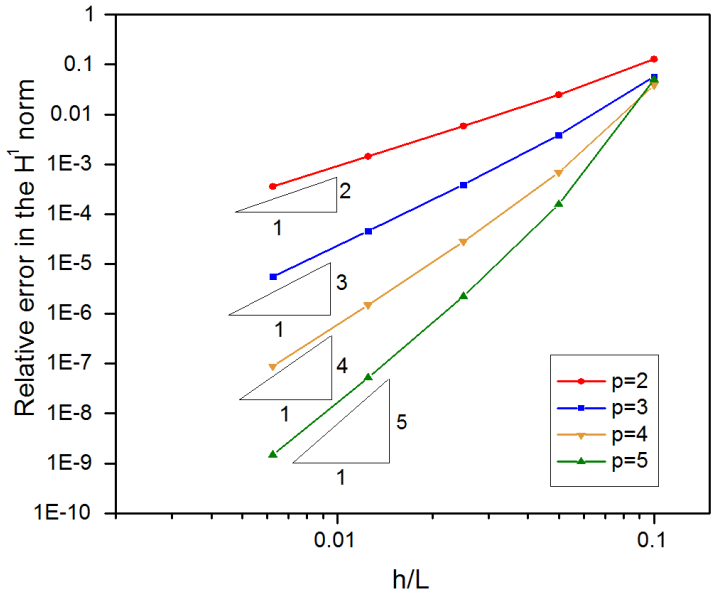

Figure 14: Singly clamped bar: Convergence of the fifth eigenmode in the H^1 norm with $g/L = 0.1, \gamma/L = 0.1$.

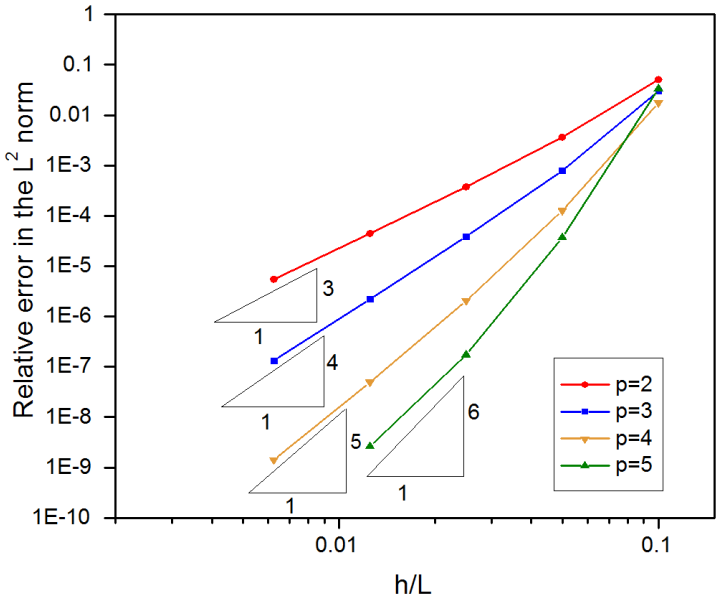

Figure 15: Singly clamped bar: Convergence of the fifth eigenmode in the L^2 norm with $g/L = 0.1, \gamma/L = 0.1$.

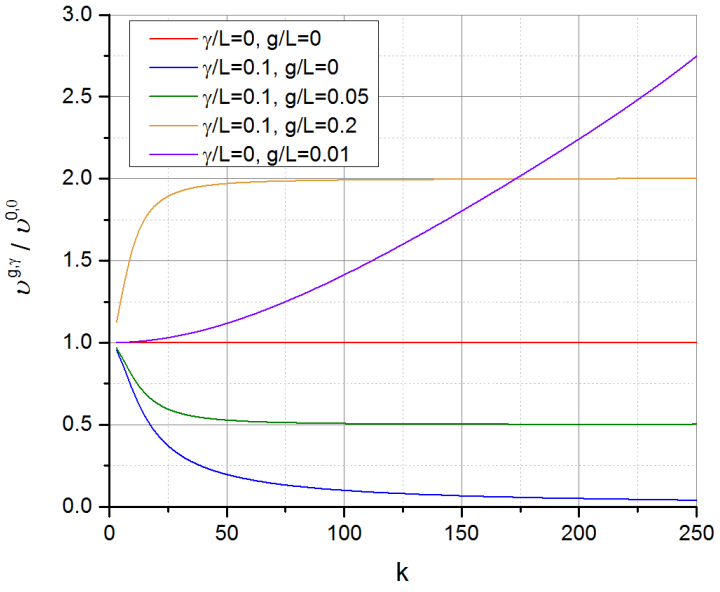

Figure 16: Singly clamped bar: Velocity ratio for different pairs of gradient parameters g and γ.

For the material values, we have used $E = 210000$ MPa and $\nu = 0.3$.

In Fig. 17, the distribution of the displacement field magnitude is shown for 64 elements with $p = q = 5$. Convergence curves for the relative error in the H^2, H^1 and L^2 norms are shown in Figs. 18,19 and 20, respectively, for $p = 2, 3, 4, 5$ with C^{p-1} continuity. As can be seen in Fig. 18, the convergence rate in the H^2 norm is of the order $\mathcal{O}(h^{p-1})$ as the theoretical results predict, whereas in the H^1 norm the convergence rate is $\mathcal{O}(h^p)$. In the L^2 norm, the convergence order for $p = 2$ is $\mathcal{O}(h^p)$, while for higher orders it is $\mathcal{O}(h^{p+1})$.

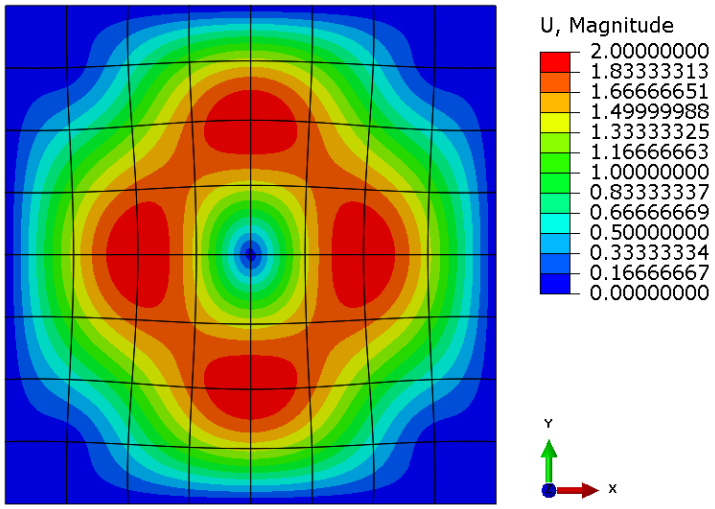

Figure 17: Singly clamped square plate: Distribution of the magnitude of the displacement field.

6.4. Benchmarks for in-plane vibrations for square and annular plates

Let us first consider a plate with square domain Ω of side length $L = 10mm$ for $g/L = 0.1$ and $\gamma/L = 0.05$. The boundary of the plate is assumed to be singly clamped in the tangential direction,

$$\boldsymbol{u} \cdot \boldsymbol{s}|_{\partial\Omega} = 0. \tag{6.14}$$

For the material values, we have used $E = 210000$ MPa and $\nu = 0.3$.

Some of the first eigenfrequencies $(1, 3, 5, 7, 10, 15)$ are presented in Table 1 for $p = 3$ and 2178 degrees of freedom, whereas the corresponding eigenmodes are depicted in Figure 21 As one can see, the gradient elasticity

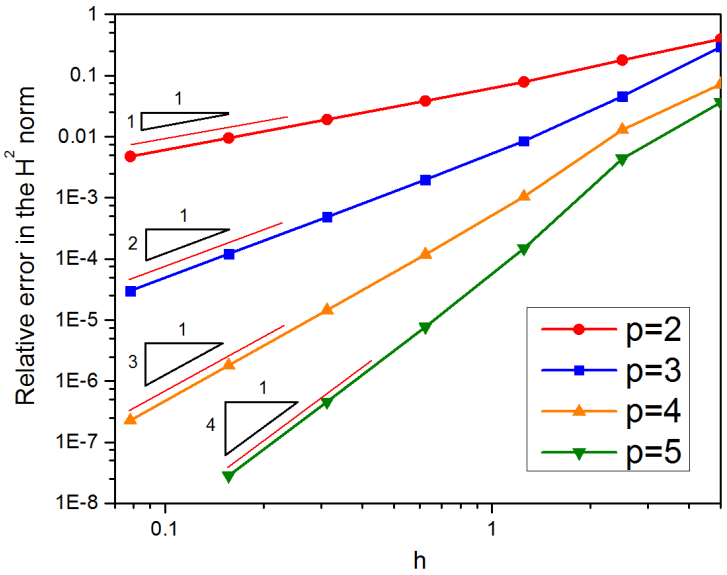

Figure 18: Singly clamped square plate: Convergence in the H^2 norm.

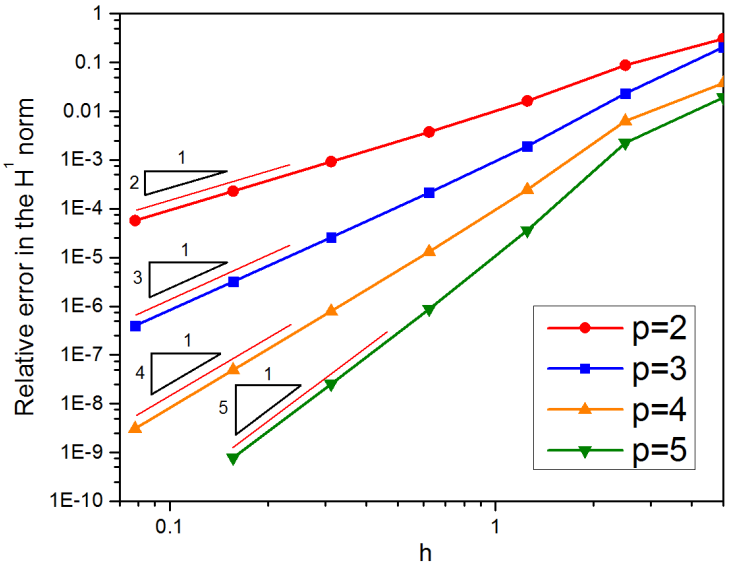

Figure 19: Singly clamped square plate: Convergence in the H^1 norm.

Table 1: Tangentially singly clamped square plate: Eigenfrequencies.

Frequency number	Frequency (Hz) Classical elasticity Numerical	Gradient elasticity Numerical	Frequency ratio Gradient/Classical
1	1.604E+5	1.661E+5	1.035
3	2.268E+5	2.401E+5	1.059
5	3.208E+5	3.614E+5	1.127
7	3.586E+5	4.087E+5	1.140
10	4.811E+5	5.981E+5	1.243
15	5.783E+5	7.344E+5	1.270

theory changes the eigenfrequencies and the ratio between the values following the classical and gradient elastic theories increases with the frequency number, from 0.68 for the 3rd mode up to 4.80 for the 20th mode.

Let us next consider an annulus plate wit domain Ω of outer radius $R = 10$ mm and inner radius $r = 5$ mm. The boundary of the domain is set to be doubly free. NURBS of order $p = 5$ are used for the computations giving C^4 continuity apart two exception lines. Namely, the geometry and mesh are formed such that the starting point is a rectangular strip with a C^0-continuous cutting line in the middle of the strip. The strip is then mapped to the shape of an annulus such that the joint line formed by the ends of the strip is C^0-continuous. Finally, C^1 continuity is build between the two C^0 border lines by combining the neighbouring degrees of freedom appropriately.

The differences between the lowest eigenfrequency of the classical elasticity and gradient elasticity are reported in Table 2 with different combinations of gradient coefficients g and γ. One can see that gradient parameters can have a dramatic effect on the frequencies. Frequency increases with the gradient parameter g, whereas with the gradient parameter γ it decreases. The lowest eigenmodes with $\gamma = 0$ and $g/a = 0, 0.6, 0.8$ and 1.0 are presented in Fig. 22 showing how the mode changes with the parameter value.

In Fig. 23, the four lowest eigenmodes (after the rigid body motions) and their frequencies for $g = 0 = \gamma$ and $g/a = 0.6, \gamma/a = 0.2$, respectively, are compared. One can clearly see that introducing the gradient parameters changes the order of modes, not the frequency values alone.

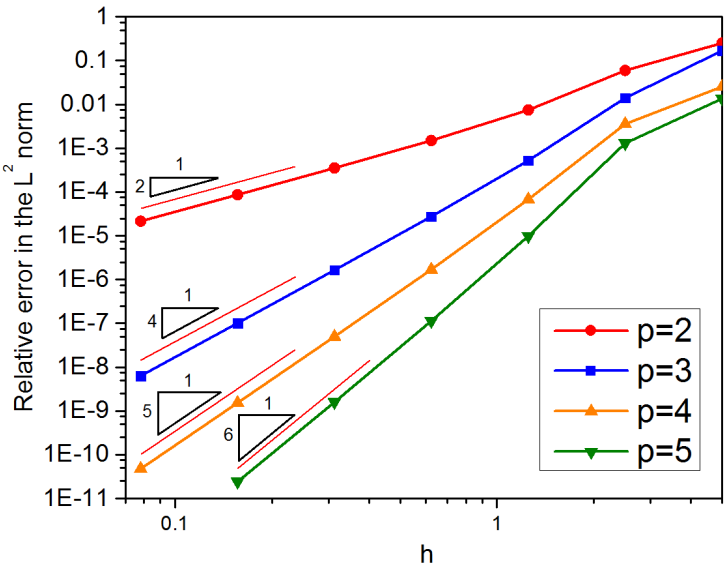

Figure 20: Singly clamped square plate: Convergence in the L^2 norm.

Table 2: Doubly free annulus plate: The lowest eigenfrequency with different gradient parameters.

g/a	γ/a	Frequency numerical (kHz)	Gradient/Classical
0	0	50.301	1
0.2	0	61.637	1.225363
0.2	0.2	60.323	1.199241
0.2	0.4	56.739	1.12799
0.2	0.6	51.776	1.029323
0.2	0.8	46.422	0.922884
0.2	1.0	41.359	0.82223
0.4	0.0	79.515	1.580784
0.6	0.0	94.437	1.877438
0.8	0.0	104.751	2.082483
1.0	0.0	111.518	2.217014

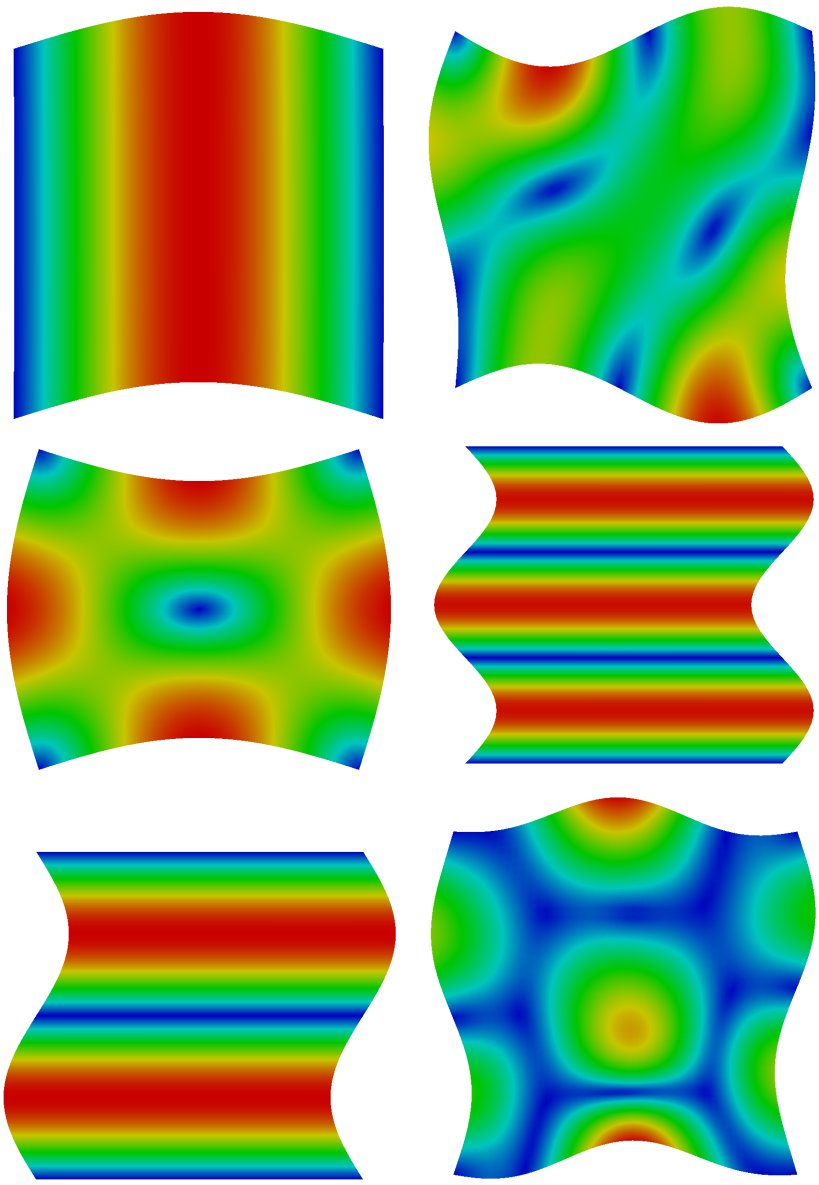

Figure 21: Tangentially singly clamped square plate: Eigenmodes $1, 3, 5$ (left) and $7, 10, 15$ (right).

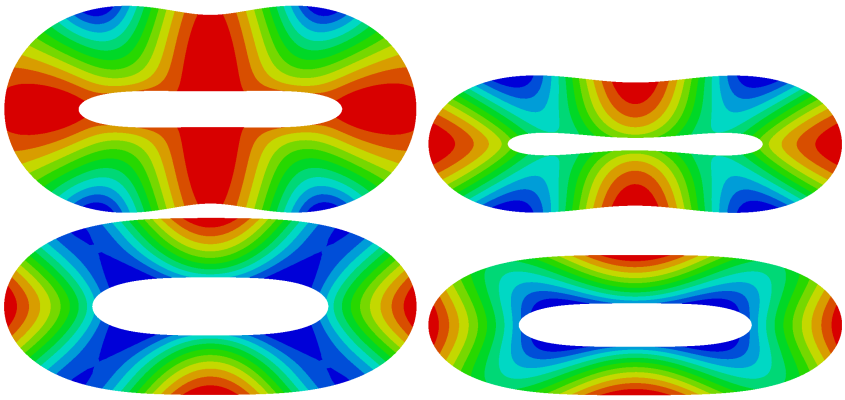

Figure 22: Doubly free annulus plate: The lowest eigenmode with $\gamma = 0$ and $g/a = 0$ (top left), $g/a = 0.6$ (top right), $g/a = 0.8$ (bottom left), $g/a = 1.0$ (bottom right).

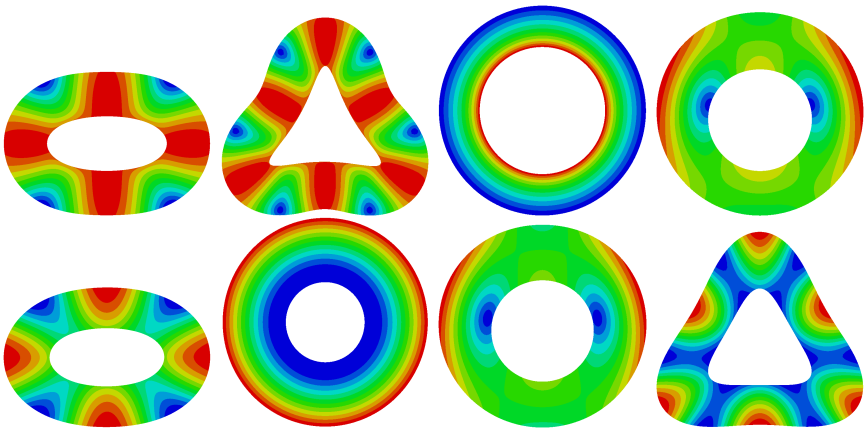

Figure 23: Doubly free annulus plate: The four lowest eigenmodes with $g = 0 = \gamma$ (top row; with frequencies $503012, 118110, 120964, 150286$ Hz) and for $g/a = 0.6, \gamma/a = 0.2$ (bottom row; with frequencies $93276, 152165, 161932, 192085$ Hz).

Acknowledgements

The first three authors has been supported by Academy of Finland through the project *Adaptive isogeometric methods for thin-walled structures* (decision number 270007). The fourth author has been supported by Academy of Finland through the project *How to handle the prima donna of structures: analysis and development of advanced discretization techniques for the simulation of thin shells* (decision number 260302).

7. Appendix

Derivation of (3.10). First, integration by parts for the classical strain energy is recalled below and then modified for the non-classical counterpart:

$$\begin{aligned}\delta W_{\text{int}}^{\text{c}} &= t\int_{\Omega}\boldsymbol{\sigma}:\boldsymbol{\varepsilon}(\delta\boldsymbol{u})\,\mathrm{d}\Omega\\ &= -t\int_{\Omega}\operatorname{div}\boldsymbol{\sigma}\cdot\delta\boldsymbol{u}\,\mathrm{d}\Omega + t\int_{\partial\Omega}\boldsymbol{\sigma}\boldsymbol{n}\cdot\delta\boldsymbol{u}\,\mathrm{d}s,\end{aligned}\tag{7.1}$$

where div denotes the standard scalar-valued divergence operator.

Second, integration by parts is applied (once) for the strain energy of the gradient-elastic augmentation:

$$\begin{aligned}\delta W_{\text{int}}^{\nabla} &= g^2 t\int_{\Omega}\boldsymbol{\nabla}\boldsymbol{\sigma}\vdots\boldsymbol{\nabla}\boldsymbol{\varepsilon}(\delta\boldsymbol{u})\,\mathrm{d}\Omega = g^2 t\int_{\Omega}\sigma_{ij,k}\epsilon_{ij,k}\,\mathrm{d}\Omega\\ &= -g^2 t\int_{\Omega}\sigma_{ij,kk}\epsilon_{ij}\,\mathrm{d}\Omega + g^2 t\int_{\partial\Omega}\sigma_{ij,k}n_k\epsilon_{ij}\,\mathrm{d}s\\ &= -g^2 t\int_{\Omega}\Delta\boldsymbol{\sigma}:\boldsymbol{\varepsilon}(\delta\boldsymbol{u})\,\mathrm{d}\Omega + g^2 t\int_{\partial\Omega}(\boldsymbol{\nabla}\boldsymbol{\sigma})\boldsymbol{n}:\boldsymbol{\varepsilon}(\delta\boldsymbol{u})\,\mathrm{d}s.\end{aligned}\tag{7.2}$$

Regarding the notation above and in what follows, we have used the Einstein summation convention. The Laplacian of the stress tensor above can be considered as a second-order tensor resulting from scalar Laplacian operating on the stress tensor, i.e., on each of its components separately. For tensor operations, we have used an abbreviation by omitting dots or other operations between tensors, except for scalar products (with one, two or three dots defined in (2.2)), whereas parentheses have been used for clarity when considered appropriate. For instance, with this notation the product $\boldsymbol{\sigma}\boldsymbol{n}$ can be naturally understood as a standard matrix vector multiplication between the (2×2) stress matrix and a (2×1) normal vector.

Remark 7. *Inserting now* (7.2) *into* (2.20) *shows that*

$$\begin{aligned}\delta W_{int} &= \delta W_{int}^{c} + \delta W_{int}^{\nabla}\\ &= t\int_{\Omega}(1-g^2\Delta)\boldsymbol{\sigma}:\boldsymbol{\varepsilon}(\delta\boldsymbol{u})\,\mathrm{d}\Omega + g^2 t\int_{\partial\Omega}(\boldsymbol{\nabla}\boldsymbol{\sigma})\boldsymbol{n}:\boldsymbol{\varepsilon}(\delta\boldsymbol{u})\,\mathrm{d}s,\end{aligned}\tag{7.3}$$

which is not identical to (2.31) *due to the augmenting boundary term resulting from integration by parts and affecting essentially the boundary conditions of the problem, as will be seen in what follows.*

Next, integration by parts will be applied for the domain integral in (7.2):

$$\delta W_{\text{int}}^{\nabla} = g^2 t \int_{\Omega} \mathbf{div}\,(\Delta\boldsymbol{\sigma}) \cdot \delta\boldsymbol{u}\,\mathrm{d}\Omega - g^2 t \int_{\partial\Omega} (\Delta\boldsymbol{\sigma})\boldsymbol{n} \cdot \delta\boldsymbol{u}\,\mathrm{d}s + g^2 t \int_{\partial\Omega} (\boldsymbol{\nabla}\boldsymbol{\sigma})\boldsymbol{n} : \boldsymbol{\varepsilon}(\delta\boldsymbol{u})\,\mathrm{d}s \tag{7.4}$$

Now, the domain integral and the first boundary integral above are of the same form as their counterparts in the classical energy expression in (7.1), i.e., the stress quantities work against the virtual displacement.

The third step is dedicated to the double-dot product in the second boundary integral of (7.4) which will be first split into the tangential and normal components and then the tangential part will be integrated by parts – by taking into account the corresponding jumps in the corners c_m of the boundary curve (derived in detail later below):

$$\begin{aligned} & g^2 t \int_{\partial\Omega} (\boldsymbol{\nabla}\boldsymbol{\sigma})\boldsymbol{n} : \boldsymbol{\varepsilon}(\delta\boldsymbol{u})\,\mathrm{d}s \\ &= g^2 t \int_{\partial\Omega} ((\boldsymbol{\nabla}\boldsymbol{\sigma})\boldsymbol{n})\boldsymbol{n} \cdot (\boldsymbol{\nabla}(\delta\boldsymbol{u}))\boldsymbol{n}\,\mathrm{d}s - g^2 t \int_{\partial\Omega} \frac{\partial((\boldsymbol{\nabla}\boldsymbol{\sigma})\boldsymbol{n})}{\partial s}\boldsymbol{s} \cdot \delta\boldsymbol{u}\,\mathrm{d}s \\ &\quad + g^2 t \int_{\partial\Omega} \kappa(s)((\boldsymbol{\nabla}\boldsymbol{\sigma})\boldsymbol{n})\boldsymbol{n} \cdot \delta\boldsymbol{u}\,\mathrm{d}s \\ &\quad + g^2 t \sum_{m=1}^{n_c} \Big(\big(((\boldsymbol{\nabla}\boldsymbol{\sigma})\boldsymbol{n}_m)\boldsymbol{s}_m - ((\boldsymbol{\nabla}\boldsymbol{\sigma})\boldsymbol{n}_{m+1})\boldsymbol{s}_{m+1} \big) \cdot \delta\boldsymbol{u} \Big)(c_m) \end{aligned} \tag{7.5}$$

where $\kappa(s)$ denotes the curvature of the boundary curve. Indeces m and $m+1$ for the normal and tangent vectors above refer to the corresponding neighboring boundary curves Γ_m and Γ_{m+1}, respectively, such that corner index n_c+1 is identified with corner index 1. We emphasize that none of the terms above have counterparts in the classical energy expression (7.1).

Remark 8. *The result in* (7.5) *giving the essentially new terms to the boundary conditions can be compared to [25] (eq. (66)) which reduces the corresponding results from the three-dimensional theory but do not identify the curvature and omit the jump terms. On the other hand, our derivation reveals*

that the last two integral terms in (7.5) *can be combined as (see Appendix)*

$$
\begin{aligned}
&- g^2 t \int_{\partial\Omega} \frac{\partial((\boldsymbol{\nabla\sigma})\boldsymbol{n})}{\partial s}\boldsymbol{s}\cdot\delta\boldsymbol{u}\,\mathrm{d}s + g^2 t\int_{\partial\Omega}\kappa(s)((\boldsymbol{\nabla\sigma})\boldsymbol{n})\boldsymbol{n}\cdot\delta\boldsymbol{u}\,\mathrm{d}s\\
&= -g^2 t\int_{\partial\Omega}\frac{\partial(((\boldsymbol{\nabla\sigma})\boldsymbol{n})\boldsymbol{s})}{\partial s}\cdot\delta\boldsymbol{u}\,\mathrm{d}s, \qquad (7.6)
\end{aligned}
$$

where the force term in the resulting integrand appears in the corner terms of (7.5) *as well.*

For deriving (7.5), we first notice that instead of using the symmetric gradient, the strain tensor $\boldsymbol{\varepsilon}$, in the integrand we can use the full gradient since the stress tensor is symmetric. Second, we split the gradient into the normal and tangential parts and hence we get

$$
\begin{aligned}
g^2 t\int_{\partial\Omega}(\nabla\boldsymbol{\sigma})\boldsymbol{n} : \boldsymbol{\varepsilon}(\delta\boldsymbol{u})\,\mathrm{d}s &= g^2 t\int_{\partial\Omega}\sigma_{ij,k}n_k\epsilon_{ij}\,\mathrm{d}s = g^2 t\int_{\partial\Omega}\sigma_{ij,k}n_k\delta u_{i,j}\,\mathrm{d}s\\
&= g^2 t\int_{\partial\Omega}\sigma_{ij,k}n_k(n_j\frac{\partial\delta u_i}{\partial n} + s_j\frac{\partial\delta u_i}{\partial s})\,\mathrm{d}s \qquad (7.7)
\end{aligned}
$$

and then focus on the tangential part. By using a shorthand notation $B_{ij} = g^2\sigma_{ij,k}n_k$ and integration by parts, we get

$$
\begin{aligned}
\int_{\partial\Omega} B_{ij}s_j\frac{\partial\delta u_i}{\partial s}\,\mathrm{d}s &= -\int_{\partial\Omega}\frac{\partial(B_{ij}s_j)}{\partial s}\delta u_i\,\mathrm{d}s\\
&\quad + \sum_{m=1}^{n_c}\Big(\big((B_{ij}s_j)_m - (B_{ij}s_j)_{m+1}\big)\delta u_i\Big)(c_m)\\
&= -\int_{\partial\Omega}\frac{\partial(\boldsymbol{Bs})}{\partial s}\cdot\delta\boldsymbol{u}\,\mathrm{d}s\\
&\quad + \sum_{m=1}^{n_c}\Big(\big((\boldsymbol{Bs})_m - (\boldsymbol{Bs})_{m+1}\big)\cdot\delta\boldsymbol{u}\Big)(c_m). \qquad (7.8)
\end{aligned}
$$

Indeces m and $m+1$ for the normal and tangent vectors above refer to the corresponding neighbouring smooth parts Γ_m and Γ_{m+1} of the boundary curve, such that corner index n_c+1 is identified with corner index 1.

The integral term in (7.8) can be split by the chain rule into two integrals:

$$
\begin{aligned}
-\int_{\partial\Omega}\frac{\partial(B_{ij}s_j)}{\partial s}\delta u_i\,\mathrm{d}s &= -\int_{\partial\Omega}\frac{\partial B_{ij}}{\partial s}s_j\delta u_i\,\mathrm{d}s - \int_{\partial\Omega}B_{ij}\frac{\partial s_j}{\partial s}\delta u_i\,\mathrm{d}s\\
&= -\int_{\partial\Omega}\big(\frac{\partial\boldsymbol{B}}{\partial s}\boldsymbol{s}\big)\cdot\delta\boldsymbol{u}\,\mathrm{d}s - \int_{\partial\Omega}\big(\boldsymbol{B}\frac{\partial\boldsymbol{s}}{\partial s}\big)\cdot\delta\boldsymbol{u}\,\mathrm{d}s, \qquad (7.9)
\end{aligned}
$$

where one can use the definition for the curvature $\kappa(s)$ of the boundary curve $\partial\Omega$ for $\partial \boldsymbol{s}/\partial s = -\kappa(s)\boldsymbol{n}$. Finally, together with the normal part of the gradient in (7.7), substituting $\boldsymbol{B}$ in (7.8) and (7.9) implies (7.5).

Proof of Theorem 1. First, for the classical part the one-dimensional Cauchy–Schwartz inequality gives the bound $a^{\mathrm{c}}(u,v) \leq |u|_1|v|_1$. Second, for the non-classical part in an analogous way, it holds that $a^{\nabla}(u,v) \leq g^2|u|_2|v|_2$. Altogether, we get the upper bound

$$a(u,v) \leq |u|_1|v|_1 + g^2|u|_2|v|_2 \leq C_1\|u\|_2\|v\|_2, \tag{7.10}$$

where $C_1 = 1+g^2$. This guarantees the continuity of the bilinear form $a(\cdot,\cdot)$ with respect to the H^2 norm.

Proof of Theorem 2. First, for the classical part we recall the elementary one-dimensional Poincaré–Friedrichs inequality in order to keep track on the constants involved in the analysis. In particular, the relations between g and L have an essential role in the model, from both physical and mathematical points of view. With $v(0) = 0$, the fundamental theorem of calculus and the Cauchy–Schwartz inequality imply that $\|v\|_0^2 \leq L^2|v|_1^2$. Hence, $\|v\|_1^2 \leq (1+L^2)|v|_1^2$ and finally

$$a^{\mathrm{c}}(v,v) = |v|_1^2 \geq \frac{1}{1+L^2}\|v\|_1^2. \tag{7.11}$$

Second, for the non-classical part it trivially holds that

$$a^{\nabla}(v,v) = g^2\int_0^L (v''(x))^2\,\mathrm{d}x = g^2|v|_2^2 \tag{7.12}$$

giving the lower bound

$$a(v,v) \geq \frac{1}{1+L^2}\|v\|_1^2 + g^2|v|_2^2 \geq \alpha_1(\|v\|_1^2 + |v|_2^2) = \alpha_1\|v\|_2^2. \tag{7.13}$$

where $\alpha_1 = \min((1+L^2)^{-1}, g^2)$. This quarantees that the bilinear form $a(\cdot,\cdot)$ is coercive over the space V endowed with the H^2 norm.

Proof of Theorem 3. By continuity and coercivity, the bilinear form $a(\cdot,\cdot)$ is an inner product on V and hence the pair $(V, a(\cdot,\cdot))$ is a Hilbert space. In addition, by the Cauchy–Schwartz inequality the load functional $l(\cdot)$ belonging to the dual space V' is linear and continuous on V:

$$l(v) = \int_\Omega f\,v\,\mathrm{d}\Omega \leq \|f\|_0\|v\|_0 \leq \|f\|_0\|v\|_2 \quad \forall v \in V. \tag{7.14}$$

Hence, Riesz Representation Theorem implies the uniqueness of the solution.

Proof of Theorem 4. First, for the classical part it holds that

$$\begin{aligned} a^{\mathrm{c}}(\boldsymbol{u},\boldsymbol{v}) &\le \max(1-\nu,\nu)\int_\Omega \big(\boldsymbol{\varepsilon}(\boldsymbol{u}):\boldsymbol{\varepsilon}(\boldsymbol{v})+(\operatorname{tr}\boldsymbol{\varepsilon}(\boldsymbol{u})\boldsymbol{I}):\boldsymbol{\varepsilon}(\boldsymbol{v})\big)\,\mathrm{d}\Omega \\ &\le 2\max(1-\nu,\nu)\,|\boldsymbol{u}|_1|\boldsymbol{v}|_1, \end{aligned} \tag{7.15}$$

where the last inequality follows from the Cauchy–Schwartz inequality and the strain definition (2.3) with the first Sobolev seminorm defined (in the Cartesian system) as

$$|\boldsymbol{v}|_1^2=\int_\Omega \boldsymbol{\nabla}\boldsymbol{v}:\boldsymbol{\nabla}\boldsymbol{v}\,\mathrm{d}\Omega=\int_\Omega \big(v_{x,x}^2+v_{x,y}^2+v_{y,x}^2+v_{y,y}^2\big)\,\mathrm{d}\Omega. \tag{7.16}$$

The first subscript above refers to the coordinate direction, while the second one after the comma indicates the partial derivatives.

Second, for the non-classical part it holds that

$$\begin{aligned} a^{\nabla}(u,v) &\le g^2\max(1-\nu,\nu)\int_\Omega \big(\boldsymbol{\nabla}\boldsymbol{\varepsilon}(\boldsymbol{u})+\boldsymbol{\nabla}(\operatorname{tr}\boldsymbol{\varepsilon}(\boldsymbol{u})\boldsymbol{I})\big)\vdots\big(\boldsymbol{\nabla}\boldsymbol{\varepsilon}(\boldsymbol{v})\big)\,\mathrm{d}\Omega \\ &\le 2g^2\max(1-\nu,\nu)\,|\boldsymbol{u}|_2|\boldsymbol{v}|_2, \end{aligned} \tag{7.17}$$

with the second Sobolev seminorm defined (in the Cartesian system) as

$$\begin{aligned} |\boldsymbol{v}|_2^2 &= \int_\Omega \boldsymbol{\nabla}(\boldsymbol{\nabla}\boldsymbol{v})\vdots\boldsymbol{\nabla}(\boldsymbol{\nabla}\boldsymbol{v})\,\mathrm{d}\Omega \\ &= \int_\Omega \big(v_{x,xx}^2+v_{y,xx}^2+2v_{x,xy}^2+2v_{y,xy}^2+v_{x,yy}^2+v_{y,yy}^2\big)\,\mathrm{d}\Omega. \end{aligned} \tag{7.18}$$

Altogether, we get the upper bound

$$a(\boldsymbol{u},\boldsymbol{v})\le 2\max(1-\nu,\nu)\big(|\boldsymbol{u}|_1|\boldsymbol{v}|_1+g^2|\boldsymbol{u}|_2|\boldsymbol{v}|_2\big)\le C_2\|\boldsymbol{u}\|_2\|\boldsymbol{v}\|_2, \tag{7.19}$$

with $C_2=2\max(1-\nu,\nu)(1+g^2)$, guaranteeing the continuity of the bilinear form $a(\cdot,\cdot)$ with respect to the H^2 norm.

Proof of Theorem 5. First, for for the classical part we recall the proof in [41] to be imitated below for the non-classical part:

$$\begin{aligned} a^{\mathrm{c}}(\boldsymbol{v},\boldsymbol{v}) &= (1-\nu)\|\boldsymbol{\varepsilon}(\boldsymbol{v})\|_0^2+\nu\,(\operatorname{tr}\boldsymbol{\varepsilon}(\boldsymbol{v}))^2 \\ &\ge (1-\nu)\|\boldsymbol{\varepsilon}(\boldsymbol{v})\|_0^2\ge\frac{1-\nu}{2}\,|\boldsymbol{v}|_1^2, \end{aligned} \tag{7.20}$$

where the last inequality follows from the ellipticity of the strain tensor proved and later imitated in the special case of homogeneous Dirichlet boundary conditions:

$$\begin{aligned}\|\boldsymbol{\varepsilon}(\boldsymbol{v})\|_0^2 &= \int_\Omega \frac{1}{2}\big(\boldsymbol{\nabla}\boldsymbol{u} + (\boldsymbol{\nabla}\boldsymbol{u})^T\big) : \frac{1}{2}\big(\boldsymbol{\nabla}\boldsymbol{u} + (\boldsymbol{\nabla}\boldsymbol{u})^T\big)\,\mathrm{d}\Omega \\ &= \frac{1}{2}\|\boldsymbol{\nabla}\boldsymbol{v}\|_0^2 + \frac{1}{2}\int_\Omega \boldsymbol{\nabla}\boldsymbol{v} : (\boldsymbol{\nabla}\boldsymbol{v})^T\,\mathrm{d}\Omega \geq \frac{1}{2}|\boldsymbol{v}|_1^2. \end{aligned} \tag{7.21}$$

The inequality above follows by applying integration by parts (twice) with functions $\boldsymbol{v} \in [C_0^\infty(\Omega)]^2$ dense in $[H_0^1(\Omega)]^2$ giving vanishing boundary integrals:

$$\begin{aligned}\int_\Omega \boldsymbol{\nabla}\boldsymbol{v} : (\boldsymbol{\nabla}\boldsymbol{v})^T\,\mathrm{d}\Omega &= -\int_\Omega \boldsymbol{v}\cdot\mathbf{div}\,((\boldsymbol{\nabla}\boldsymbol{v})^T)\,\mathrm{d}\Omega + \int_{\partial\Omega}\boldsymbol{v}\cdot(\boldsymbol{\nabla}\boldsymbol{v})^T\boldsymbol{n}\,\mathrm{d}\Omega \\ &= \int_\Omega (\operatorname{div}\boldsymbol{v})^2\,\mathrm{d}\Omega \geq 0. \end{aligned} \tag{7.22}$$

Second, for the non-classical part, in turn, we write out the triple dot product in an analogous way:

$$\begin{aligned}a^\nabla(v,v) &= (1-\nu)\|\boldsymbol{\nabla}\boldsymbol{\varepsilon}(\boldsymbol{v})\|_0^2 + \nu\int_\Omega |\boldsymbol{\nabla}((\operatorname{tr}\boldsymbol{\varepsilon})\boldsymbol{I})|^2\,\mathrm{d}\Omega \\ &\geq (1-\nu)\|\boldsymbol{\nabla}\boldsymbol{\varepsilon}(\boldsymbol{v})\|_0^2 \geq \frac{1-\nu}{2}|\boldsymbol{v}|_2^2, \end{aligned} \tag{7.23}$$

where the last inequality follows from the inequality below:

$$\begin{aligned}\|\boldsymbol{\nabla}\boldsymbol{\varepsilon}(\boldsymbol{v})\|_0^2 &= \frac{1}{2}\|\boldsymbol{\nabla}(\boldsymbol{\nabla}\boldsymbol{v})\|_0^2 + \frac{1}{2}\int_\Omega \boldsymbol{\nabla}(\boldsymbol{\nabla}\boldsymbol{v}) \vdots \boldsymbol{\nabla}((\boldsymbol{\nabla}\boldsymbol{v})^T)\,\mathrm{d}\Omega \\ &\geq \frac{1}{2}\|\boldsymbol{\nabla}(\boldsymbol{\nabla}\boldsymbol{v})\|_0^2 = \frac{1}{2}|\boldsymbol{v}|_2^2. \end{aligned} \tag{7.24}$$

The inequality above follows by applying integration by parts (twice) for the last integral expression above:

$$\int_\Omega \boldsymbol{\nabla}(\boldsymbol{\nabla}\boldsymbol{v}) \vdots \boldsymbol{\nabla}((\boldsymbol{\nabla}\boldsymbol{v})^T)\,\mathrm{d}\Omega = \int_\Omega |\nabla(\operatorname{div}\boldsymbol{v})|^2\,\mathrm{d}\Omega, \tag{7.25}$$

It should be noticed that the boundary integrals of the integration by parts above have vanished: if the boundary is smooth, the resulting jump terms

vanish; if the domain is convex and the boundary is Lipschitz-continuous, the jump terms vanish since the trace of $v_i \in H^2(\Omega)$ is continuous ($H^2(\Omega)$ is compactly embedded in $C(\bar{\Omega})$ by Sobolev's inequality [49]).

Altogether, we get the lower bound

$$\begin{aligned} a(\boldsymbol{v},\boldsymbol{v}) &\geq \frac{1-\nu}{2}(|\boldsymbol{v}|_1^2 + g^2|\boldsymbol{v}|_2^2) \\ &\geq \frac{1-\nu}{2}((1+\operatorname{diam}(\Omega))^{-2}\|\boldsymbol{v}\|_1^2 + g^2|\boldsymbol{v}|_2^2) \geq \alpha_2\|v\|_2^2, \end{aligned} \tag{7.26}$$

where the second inequality follows from the Poincaré–Friedrichs inequality [39] and $\alpha_2 = \min((1+\operatorname{diam}(\Omega))^{-2}, g^2)(1-\nu)/2$. This quarantees that the bilinear form $a(\cdot,\cdot)$ is coercive over the space $\boldsymbol{V}$ endowed with the H^2 norm.

Proof of Theorem 6. The proof is analogous to the one of Theorem 3.

References

[1] G. A. Maugin, Generalized continuum mechanics: What do we mean by that?, in: G. A. Maugin, A. V. Metrikine (Eds.), Mechanics of Generalized Continua, One Hundred Years After the Cosserats, Springer, 2010, pp. 3–14.

[2] G. A. Maugin, A historical perspective of generalized continuum mechanics, in: H. Altenbach, G. A. Maugin, V. Erofeev (Eds.), Mechanics of Generalized Continua, Springer, 2011, pp. 3–14.

[3] H. Askes, E. C. Aifantis, Gradient elasticity in statics and dynamics: An overview of formulations, length scale identification procedures, finite element implementations and new results, International Journal of Solids and Structures 48 (2011) 1962–1990.

[4] E. C. Aifantis, On the role of gradients in the localization of deformation and fracture, International Journal of Engineering Science 30 (1992) 1279–1299.

[5] B. S. Altan, E. C. Aifantis, On the structure of the mode III crack-tip in gradient elasticity, Scripta Mellurgica et Materialia 26 (1992) 319–324.

[6] R. D. Mindlin, Micro-structure in linear elasticity, Archive for Rational Mechanics and Analysis 16 (1964) 51–78.

[7] R. Maranganti, P. Sharma, A novel atomistic approach to determine strain-gradient elasticity constants: Tabulation and comparison for various metals, semiconductors, silica, polymers and the (Ir) relevance for nanotechnologies, Journal of the Mechanics and Physics of Solids 55 (2007) 1823–1852.

[8] E. C. Aifantis, Exploring the applicability of gradient elasticity to certain micro/nano reliability problems, Microsystem Technologies 15 (2009) 109–115.

[9] K. A. Lazopoulos, On the gradient strain elasticity theory of plates, European Journal of Mechanics A/Solids 23 (2004) 843–852.

[10] D. C. C. Lam, F. Yang, A. C. M. Chong, J. Wang, P. Tong, Experiments and theory in strain gradient elasticity, Journal of the Mechanics and Physics of Solids 51 (2003) 1477–1508.

[11] M. Malagú, E. Benvenuti, A. Simone, One-dimensional nonlocal elasticity for tensile single-walled carbon nanotubes: A molecular structural mechanics characterization, European Journal of Mechanics A/Solids 54 (2015) 160–170.

[12] K. A. Lazopoulos, Static and dynamic analysis of a gradient-elastic bar in tension, Archive of Applied Mechanics 72 (2002) 483–497.

[13] S. Papargyri-Beskou, D. Polyzos, D. E. Beskos, Wave dispersion in gradient elastic solids and structures: A unified treatment, International Journal of Solids and Structures 40 (2009) 385–400.

[14] T. J. R. Hughes, J. A. Cottrell, Y. Bazilevs, Isogeometric analysis: CAD, finite elements, NURBS, exact geometry and mesh refinement, Comput. Methods Appl. Mech. Engrg. 194 (2005) 4135–4195.

[15] J. Kiendl, K.-U. Bletzinger, J. Linhard, R. Wüchner, Isogeometric shell analysis with Kirchhoff–Love elements, Comp. Meths. Appl. Mech. Engrg. 198 (2010) 3902–3914.

[16] P. Fischer, M. Klassen, J. Mergheim, P. Steinmann, R. Müller, Isogeometric analysis of 2D gradient elasticity, Computational Mechanics 47 (2011) 325–334.

[17] J. Kiendl, F. Auricchio, T. Hughes, A. Reali, Single-variable formulations and isogeometric discretizations for shear deformable beams, Comp. Meths. Appl. Mech. Engrg. 284 (2015) 988–1004.

[18] L. Beirão da Veiga, T. Hughes, J. Kiendl, C. Lovadina, J. Niiranen, A. Reali, H. Speleers, A locking-free model for Reissner–Mindlin plates: Analysis and isogeometric implementation via NURBS and triangular NURPS, Math. Meth. Apll. Sci. 25 (2015) 1519–1551.

[19] F. Auricchio, L. Beirão da Veiga, A. Buffa, C. Lovadina, A. Reali, G. Sangalli, A fully locking-free isogeometric approach for plane linear elasticity problems: A stream function formulation, Comp. Meths. Appl. Mech. Engrg. 197 (2007) 160–172.

[20] L. Beirão da Veiga, A. Buffa, C. Lovadina, M. Martinelli, G. Sangalli, An isogeometric method for the Reissner–Mindlin plate bending problem, Comp. Meths. Appl. Mech. Engrg. 209–212 (2012) 450–53.

[21] H. Askes, A. S. J. Suiker, L. J. Sluys, A classification of higher-order strain-gradient models – linear analysis, Archive of Applied Mechanics 72 (2002) 171–188.

[22] B. S. Altan, E. C. Aifantis, On some aspects in the special theory of gradient elasticity, Journal of the Mechanical Behavior of Materials 8 (1997) 231–282.

[23] S. I. Markolefas, D. A. Tsouvalas, G. I. Tsamasphyros, Theoretical analysis of a class of mixed, C^0 continuity formulations for general dipolar Gradient Elasticity boundary value problems, International Journal of Solids and Structures 44 (2007) 546–572.

[24] S. Papargyri-Beskou, , D. Beskos, Static analysis of gradient elastic bars, beams, plates and shells, The Open Mechanics Journal 4 (2010) 65–73.

[25] N. Aravas, Plane-strain problems for a class of gradient elasticity models—a stress function approach, Journal of Elasticity 104 (2011) 45–70.

[26] X.-L. Gao, S. Park, Variational formulation of a simplified strain gradient elasticity theory and its application to a pressurized thick-walled

cylinder problem, International Journal of Solids and Structures 44 (2007) 7486–7499.

[27] E. Amanatidou, N. Aravas, Mixed finite element formulations of strain-gradient elasticity problems, Comp. Meths. Appl. Mech. Engrg. 191 (2002) 1723–1751.

[28] G. Engel, K. Garikipati, T. J. R. Hughes, M. G. Larson, L. Mazzei, R. L. Taylor, Continuous/discontinuous finite element approximations of fourth-order elliptic problems in structural and continuum mechanics with applications to thin beams and plates, and strain gradient elasticity, Comp. Meths. Appl. Mech. Engrg. 191 (2002) 3669–3750.

[29] A. Zervos, Finite elements for elasticity with microstructure and gradient elasticity, Int. J. Num. Meths. Eng. 73 (2008) 564–595.

[30] A. Zervos, S.-A. Papanicolopulos, I. Vardoulakis, Two finite-element discretizations for gradient elasticity, J. Eng. Mech. 135 (2009) 203–213.

[31] H. Askes, I. Morata, E. C. Aifantis, Finite element analysis with staggered gradient elasticity, Comp. Struct. 86 (2008) 1266–1279.

[32] S. Rudraraju, A. V. der Ven, K. Garikipati, Three-dimensional isogeometric solutions to general boundary value problems of Toupin's gradient elasticity theory at finite strains, Comp. Meths. Appl. Mech. Engrg. 278 (2014) 705–728.

[33] R. A. Toupin, Elastic materials with couple-stresses, Archive for Rational Mechanics and Analysis 11 (1962) 385–413.

[34] J. L. Bleustein, A note on the boundary conditions of Toupin's strain-gradient theory, International Journal of Solids and Structures 3 (1967) 1053–1057.

[35] C. Q. Ru, E. C. Aifantis, A simple approach to solve boundary-value problems in gradient elasticity, Acta Mechanica 101 (1993) 59–68.

[36] R. D. Mindlin, Second gradient of strain and surface-tension in linear elasticity, International Journal of Solids and Structures 1 (1965) 417–438.

[37] J. Niiranen, A. H. Niemi, Variational formulation and general boundary conditions for sixth order boundary value problems of gradient-elastic Kirchhoff plates, in revision for European Journal of Mechanics A/Solids.

[38] A. K. Singh, Mechanics of Solids, PHI Learning Private Limited, New Delhi, 2012.

[39] D. Braess, Finite Elements. Theory, fast solvers, and applications in solid mechanics, Cambridge University Press, Cambridge, 2001.

[40] R. A. Adams, J. Fournier, Cone conditions and properties of Sobolev spaces, Journal of Mathematical Analysis and Applications 61 (1977) 713–734.

[41] J. Nečas, I. Hlaváček, Mathematical Theory of Elastic and Elasto-Plastic Bodies: An Introduction, Elsevier, Amsterdam, 1981.

[42] R. W. Soutas-Little, Elasticity, Prentice-Hall Inc., Englewooods Cliffs, 1973.

[43] L. Beirão da Veiga, A. Buffa, J. Rivas, G. Sangalli, Some estimates for h-p-k-refinement in Isogeometric Analysis, Numer.Math. 118 (2011) 271–305.

[44] R. Stenberg, On some techniques for approximating boundary conditions in the finite element method, J. Comp. Appl. Math. 63 (1995) 139–148.

[45] L. Beirão da Veiga, J. Niiranen, R. Stenberg, A family of C^0 finite elements for Kirchhoff plates I: Error analysis, SIAM J. Num. Anal. 45 (2007) 2047–2071.

[46] L. Beirão da Veiga, J. Niiranen, R. Stenberg, A family of C^0 finite elements for Kirchhoff plates II: Numerical results, Comp. Meths. Appl. Mech. Engrg. 197 (2008) 1850–1864.

[47] Y. Bazilevs, L. Beirão da Veiga, J. A. Cottrell, T. J. R. Hughes, G. Sangalli, Isogeometric analysis: approximation, stability and error estimates for h-refined meshes, Mathematical Models and Methods in Applied Sciences 16 (2006) 1031–1090.

[48] L. Beirão da Veiga, D. Cho, G. Sangalli, Anisotropic NURBS approximation in isogeometric analysis, Comput. Methods Appl. Mech. Engrg. 209-212 (2012) 1–11.

[49] S. C. Brenner, L. R. Scott, The Mathematical Theory of Finite Element Methods, Springer, New York, 2008.

[50] M. Lyly, J. Niiranen, R. Stenberg, A refined error analysis of MITC plate elements, Math. Mod. Meth. Appl. Sci. 16 (2006) 967–977.

[51] C. de Falco, A. Reali, R. Vázquez, GeoPDEs: A research tool for Isogeometric Analysis of PDEs, Advances in Engineering Software 42 (2011) 1020–1034.

[52] S. Dassault Systemes, ABAQUS Analysis User's Guide, 32.15 User-defined elements, `http://50.16.225.63/v6.14/books/usb/default.htm` (2015).

[53] S. Khakalo, J. Niiranen, Isogeometric analysis of higher-order gradient elasticity problems by user elements of a commercial finite element software, in revision for Computer-Aided Design.

[54] T. Hughes, A. Reali, G. Sangalli, Duality and unified analysis of discrete approximations in structural dynamics and wave propagation: Comparison of p-method finite elements with k-method NURBS, Comp. Meths. Appl. Mech. Engrg. 197 (2008) 4104–4124.